Journal of
Mechanics of
Materials and Structures

CONTACT STRESS ON A ROTATING ELASTIC BAND SAW BLADE USING THE THEORY OF A COSSERAT SURFACE

M. B. Rubin and E. Tufekci

Volume 1, Nº 8 October 2006

mathematical sciences publishers

JOURNAL OF MECHANICS OF MATERIALS AND STRUCTURES
Vol. 1, No. 8, 2006

CONTACT STRESS ON A ROTATING ELASTIC BAND SAW BLADE USING THE THEORY OF A COSSERAT SURFACE

M. B. RUBIN AND E. TUFEKCI

The value of the contact stress between a band saw blade and the driving wheel is modeled using the theory of an elastic Cosserat surface. Specifically, we use nonlinear Cosserat theory to model the bending of an elastic plate into a rotating right circular cylindrical tube with associated end moments. The resulting equations are then linearized, the end moments are relieved and the reference length of the plate is adjusted to cause contact of the blade with the wheel. The results indicate that the nonuniformity in the deformed shape of the saw blade significantly influences the predictions of the value and distribution of the contact stress between the blade and the wheel even though the blade is thin. This is in addition to the influence of a crowned wheel, and the deformed shape due to the tensioning process, which are typically used to help control tracking of the blade on the wheel. Also, we showed that the value of this contact stress predicted by a simple Lamé type solution remains about 50% of that predicted by the Cosserat solution and that the effect of the rotational speed of the wheel is negligible for typical operating conditions of thin wood-cutting saws.

1. Introduction

A typical band saw blade is a thin steel strip that has been bent into a cylindrical shell with gullets cut out on one of the edges to create teeth. The blade is positioned over two rotating wheels that are separated by a controlled distance. To prevent catastrophic damage to the teeth and the wheel, the blade is only in partial contact with each wheel so that the teeth can hang freely over the edge of the wheel (Figure 1). Tension in the blade can be controlled by adjusting the positions of the wheels. Although in practice the force between the band wheels is controlled, the model used here treats the distance between the wheels as displacement controlled instead of load controlled.

A recent review of mechanical problems relating to aluminum-cutting high-speed band saws in [Gendraud et al. 2003] describes problems which reduce the quality of the surface of the material being cut, reduce the precision of the dimensions of the cut, and shorten the life of the saw blade. In other studies, attention has been focused on saw vibrations [Mote Jr. 1965; Mote and Naguleswaran 1966; Le-Ngoc and McCallion 1999; Damaren and Le-Ngoc 2000; Gendraud et al. 2003; Kong and Parker 2005] and tracking of the blade on the wheels [Wong and Schajer 1997; Wong and Schajer 2002; Barcik 2003]. Tracking of the blade can be significantly influenced by the contact stress distribution between the blade and the wheel. In practice, contact stress is modified by using a crowned wheel and by a roll tensioning process which changes the unloaded shape of the blade. Two narrow crowned rollers are used to squeeze the blade, causing plastic deformations and residual stresses. These residual stresses cause the unloaded blade to attain a deformed shape that can be optimized to help control tracking on the wheel. [Lister and

Keywords: band saw blade, Cosserat surface, contact stress, elastic.

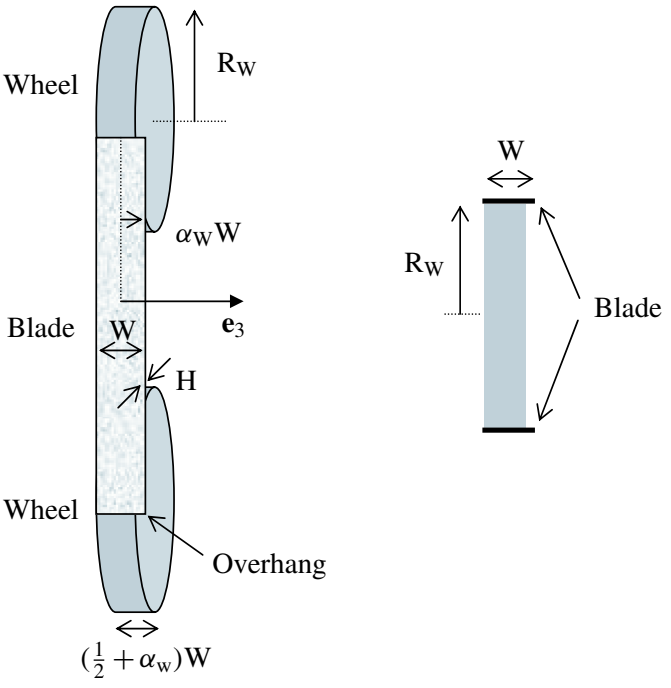

Figure 1. Sketch of the geometry of the saw blade and wheel.

Schajer 1993] analyzed this effect using plate theory. Complete elastic-plastic analysis of a saw blade remains a difficult problem because the blade experiences finite rotations and is only in partial contact with the wheels. The objective of this study is to analyze the contact stress and deformations of the rotating band saw blade. Here, a formulation is proposed which can be used to model the effects of a crowned wheel and the tensioning process. Although these effects are significant, we first concentrate on the contact stress distribution caused by nonuniform shape of the blade when a plate is deformed elastically and joined at its edges to form the blade.

In the analysis of contact stress, the straight portions of the blade are ignored and the blade is modeled as a circular cylindrical shell that is stretched and placed in partial axial contact with a circular wheel (Figure 1). The blade is considered to be a plate in its stress-free reference configuration. This plate is then deformed into an axisymmetric shell which is joined perfectly at its seam. The deformation causes circumferential tension near the blade's outer surface and circumferential compression near its inner surface. If the deformed plate (blade) were to remain a right-circular cylinder then the Poisson effect would require nonzero moments to be applied to the axial edges of the blade. However, when these edge moments are relieved and the surfaces and edges of the blade are stress-free, the blade deforms so that its mean radius is not uniform along its axes of symmetry. Consequently, the contact stress between the blade and the wheel is influenced by this prestressed state. These nonuniform deformations are in addition to those that are caused by the tensioning process described earlier. Also, the effect of the angular velocity of the wheel is shown to be negligible for typical operating conditions of wood-cutting saws.

To model the finite deformation of the plate into the axisymmetric shell and the finite rotations of the deformed blade it is necessary to use a nonlinear shell theory. Moreover, it is well known that contact problems of thin structures need to use enhanced theories which model normal extension, that is, changes in thickness, and shear deformation of the structure (for example, [Naghdi and Rubin 1989]). Here, the blade is modeled using the theory of a Cosserat surface of [Naghdi 1972; Rubin 2000]. However, to determine the deformed shape of the blade and the distribution of contact stress the nonlinear equations are linearized about a finitely deformed state.

An outline of this paper is as follows. Section 2 is a brief summary of the nonlinear Cosserat equations, and Section 3 describes a simple finite deformation solution. Section 4 develops approximate equations linearized about the solution in Section 3, and Section 5 describes the procedure used to obtain an analytical solution of these linear equations. Section 6 is a discussion of the results, Appendix A includes further details of the solution and Appendix B shows a Lamé type solution.

Throughout the text, bold-faced symbols are used to denote vector and tensor quantities. Also, $\boldsymbol{I}$ denotes the unity tensor; $\text{tr}(\boldsymbol{A})$ denotes the trace of the second order tensor $\boldsymbol{A}$ and $\boldsymbol{A}^T$ denotes the transpose of $\boldsymbol{A}$. The scalar $\boldsymbol{a}\cdot\boldsymbol{b}$ denotes the dot product between two vectors $\boldsymbol{a}$, $\boldsymbol{b}$; the scalar $\boldsymbol{A}\cdot\boldsymbol{B} = \text{tr}(\boldsymbol{A}\boldsymbol{B}^T)$ denotes the dot product between two second order tensors $\boldsymbol{A}$, $\boldsymbol{B}$; the vector $\boldsymbol{a}\times\boldsymbol{b}$ denotes the cross product between $\boldsymbol{a}$ and $\boldsymbol{b}$; and the second order tensor $\boldsymbol{a}\otimes\boldsymbol{b}$ denotes the tensor product between $\boldsymbol{a}$ and $\boldsymbol{b}$. The usual summation convention over repeated lower cased indices is implied. The range of Latin indices is (1, 2, 3) and Greek indices is (1, 2). A glossary of notation is included at the end of this paper.

2. A brief summary of the nonlinear Cosserat equations

The theory of a Cosserat surface, which is a model for a shell-like body, has been described in detail in [Naghdi 1972]. This theory is sufficiently general to model normal extension and shear deformation. Here, we make use of the formulation and notation presented in [Rubin 2000]. Specifically, the kinematics of the shell's stress-free reference configuration are characterized by

$$\big\{\boldsymbol{X}(\theta^\alpha),\, \boldsymbol{D}_3(\theta^\alpha)\big\},$$

where $\boldsymbol{X}$ locates a material point relative to a fixed origin, the director vector $\boldsymbol{D}_3$ models a material fiber through the shell's thickness, and θ^α, $(\alpha = 1, 2)$, are convected Lagrangian coordinates. Similarly, the kinematics of the shell's present deformed configuration are characterized by

$$\big\{\boldsymbol{x}(\theta^\alpha, t),\, \boldsymbol{d}_3(\theta^\alpha, t)\big\},$$

where t denotes time. Also, the tangent vectors $\boldsymbol{D}_\alpha$, $\boldsymbol{d}_\alpha$, and the directors $\boldsymbol{D}_3$, $\boldsymbol{d}_3$ are defined such that

$$\boldsymbol{D}_\alpha = \boldsymbol{X}_{,\alpha}\,, \qquad D^{1/2} = \boldsymbol{D}_1\times\boldsymbol{D}_2\cdot\boldsymbol{D}_3 > 0,$$
$$\boldsymbol{d}_\alpha = \boldsymbol{x}_{,\alpha}\,, \qquad d^{1/2} = \boldsymbol{d}_1\times\boldsymbol{d}_2\cdot\boldsymbol{d}_3 > 0,$$

where a comma denotes partial differentiation with respect to θ^α. Moreover, it is convenient to introduce the reciprocal vectors $\boldsymbol{D}^i$ and $\boldsymbol{d}^i$ by the expressions

$$\boldsymbol{D}^i\cdot\boldsymbol{D}_j = \delta^i_j, \qquad \boldsymbol{d}^i\cdot\boldsymbol{d}_j = \delta^i_j,$$

where δ^i_j is the Kronecker delta symbol. For elastic shells it is convenient to define the additional kinematic variables

$$\boldsymbol{F} = \boldsymbol{d}_i \otimes \boldsymbol{D}^i, \qquad \boldsymbol{C} = \boldsymbol{F}^T \boldsymbol{F}, \qquad \boldsymbol{E} = \tfrac{1}{2}(\boldsymbol{C} - \boldsymbol{I}), \qquad \boldsymbol{\beta}_\alpha = \boldsymbol{F}^{-1}\boldsymbol{d}_{3,\alpha} - \boldsymbol{D}_{3,\alpha},$$

where $\boldsymbol{F}$ is similar to a deformation gradient, $\boldsymbol{E}$ is similar to a Lagrangian strain tensor and $\boldsymbol{\beta}_\alpha$ are measures of inhomogeneous deformation.

Using the direct approach to the Cosserat theory [Rubin 2000, p. 91], the equations of motion of the shell can be written in the forms

$$m(\dot{\boldsymbol{v}} + y^3 \dot{\boldsymbol{w}}_3) = m\boldsymbol{b} + \boldsymbol{t}^\alpha{}_{,\alpha}, \tag{2–1a}$$

$$m(y^3 \dot{\boldsymbol{v}} + y^{33} \dot{\boldsymbol{w}}_3) = m\boldsymbol{b}^3 - \boldsymbol{t}^3 + \boldsymbol{m}^\alpha{}_{,\alpha}, \tag{2–1b}$$

where a superposed dot denotes material time differentiation holding θ^α fixed. Here, (2–1a) represents the balance of linear momentum and (2–1b) represents the balance of director momentum which can be related to a weighted average over the thickness of the shell of the three-dimensional balance of linear momentum. The balance of angular momentum is satisfied by the constitutive equations which require a second order tensor $\boldsymbol{T}$ to be symmetric. Also, m is related to the mass of the shell, $\{y^3, y^{33}\}$ are constant director inertia coefficients, the velocity $\boldsymbol{v}$ and director velocity $\boldsymbol{w}_3$ are defined by

$$\boldsymbol{v} = \dot{\boldsymbol{x}}, \qquad \boldsymbol{w}_3 = \dot{\boldsymbol{d}}_3,$$

the quantities $\{\boldsymbol{b}, \boldsymbol{b}^3\}$ are assigned fields due to body force and contact stresses on the shell's major surfaces, and constitutive equations need to be supplied for the quantities $\{\boldsymbol{t}^i, \boldsymbol{m}^\alpha\}$.

For the problem under consideration in this paper the stress-free reference configuration of the shell is taken to be a flat plate of uniform thickness H, with length L and width W defined by

$$\begin{aligned}
&\boldsymbol{X} = \theta^1 \boldsymbol{e}_2 + \theta^2 \boldsymbol{e}_z, && \boldsymbol{D}_3 = \boldsymbol{D}^3 = \boldsymbol{e}_1, && \boldsymbol{e}_z = \boldsymbol{e}_3,\\
&\theta^2 = Z, && 0 \le \theta^1 \le L, && -\tfrac{W}{2} \le Z \le \tfrac{W}{2},\\
&\boldsymbol{D}_1 = \boldsymbol{D}^1 = \boldsymbol{e}_2, && \boldsymbol{D}_2 = \boldsymbol{D}^2 = \boldsymbol{e}_z, && A^{1/2} = D^{1/2} = 1,
\end{aligned}$$

where $\boldsymbol{e}_i$ are rectangular Cartesian base vectors and the directions are specified for later convenience in describing the deformed axisymmetric shell.

Now, for a plate made from a uniform homogeneous elastic material the inertia quantities are specified by [Rubin 2000, p. 167], as

$$m = \rho_0^* H, \qquad y^3 = 0, \qquad y^{33} = \tfrac{H^2}{\pi^2},$$

where ρ_0^* is the reference mass density of the material, and the strain energy function, from [Rubin 2000, pp. 168-169] is

$$
\begin{aligned}
m\Sigma &= \frac{\mu^* H}{1-2\nu^*}\,(\nu^*(\boldsymbol{E}\cdot\boldsymbol{I})^2 + (1-2\nu^*)\boldsymbol{E}\cdot\boldsymbol{E}) + \tfrac{1}{2}H\boldsymbol{K}^{\alpha\beta}\cdot(\boldsymbol{\beta}_\alpha\otimes\boldsymbol{\beta}_\beta),\\
\boldsymbol{K}^{11} &= \frac{H^2\mu^*}{12}\left(\Big(\frac{2}{1-\nu^*}\Big)\boldsymbol{e}_2\otimes\boldsymbol{e}_2 + \boldsymbol{e}_z\otimes\boldsymbol{e}_z\right),\\
\boldsymbol{K}^{12} &= \frac{H^2\mu^*}{12}\left(\Big(\frac{2\nu^*}{1-\nu^*}\Big)\boldsymbol{e}_2\otimes\boldsymbol{e}_z + \boldsymbol{e}_z\otimes\boldsymbol{e}_2\right),\\
\boldsymbol{K}^{21} &= \frac{H^2\mu^*}{12}\left(\boldsymbol{e}_2\otimes\boldsymbol{e}_z + \Big(\frac{2\nu^*}{1-\nu^*}\Big)\boldsymbol{e}_z\otimes\boldsymbol{e}_2\right),\\
\boldsymbol{K}^{22} &= \frac{H^2\mu^*}{12}\left(\boldsymbol{e}_2\otimes\boldsymbol{e}_2 + \Big(\frac{2}{1-\nu^*}\Big)\boldsymbol{e}_z\otimes\boldsymbol{e}_z\right),
\end{aligned}
$$

where the constants $\{\mu^*, \nu^*\}$ are the shear modulus and the Poisson's ratio of the elastic material in the small deformation limit, respectively. The constitutive equations become

$$
\begin{aligned}
\boldsymbol{m}^\alpha &= H\boldsymbol{K}^{\alpha\beta}\boldsymbol{\beta}_\beta,\\
\boldsymbol{t}^i &= \frac{\mu^* H}{1-2\nu^*}\boldsymbol{F}\big(\nu^*(\boldsymbol{E}\cdot\boldsymbol{I})\boldsymbol{I} + (1-2\nu^*)\boldsymbol{E}\big)\boldsymbol{D}^i - \boldsymbol{m}^\alpha(\boldsymbol{d}_{3,\alpha}\cdot\boldsymbol{d}^i).
\end{aligned}
$$

For the problem under consideration the body force is neglected, the outer surface of the deformed shell remains traction free, and its inner surface is free to slip over the wheel but is subjected to a normal contact stress q, which is positive in compression, in regions that make contact with the wheel. Under these conditions the assigned fields $\{\boldsymbol{b}, \boldsymbol{b}^3\}$ are specified by [Rubin 2000, p. 167], now modified to include the function $f_r(Z)$ associated with a localized moment, to model effects of the tensioning process as

$$
\begin{aligned}
m\boldsymbol{b} &= q\big(\boldsymbol{x} - \tfrac{H}{2}\boldsymbol{d}_3\big)_{,1}\times\big(\boldsymbol{x} - \tfrac{H}{2}\boldsymbol{d}_3\big)_{,2},\\
m\boldsymbol{b}^3 &= \tfrac{qH}{2}\big(\boldsymbol{x} - \tfrac{H}{2}\boldsymbol{d}_3\big)_{,1}\times\big(\boldsymbol{x} - \tfrac{H}{2}\boldsymbol{d}_3\big)_{,2} + f_r(Z)\boldsymbol{e}_r,
\end{aligned}
$$

Next, the plate is deformed into an axisymmetric shell such that the deformed kinematics are

$$
\begin{aligned}
\boldsymbol{x} &= r(Z)\boldsymbol{e}_r(\theta) + z(Z)\boldsymbol{e}_z, \quad \theta = \frac{\theta^1}{R} + \omega t,\\
R &= \frac{L}{2\pi},\\
\boldsymbol{d}_3 &= \phi_r(Z)\boldsymbol{e}_r(\theta) + \phi_z(Z)\boldsymbol{e}_z,\\
\dot{\boldsymbol{v}} &= -r\omega^2\boldsymbol{e}_r,\\
\dot{\boldsymbol{w}}_3 &= -\phi_r\omega^2\boldsymbol{e}_r,
\end{aligned}
\tag{2–2}
$$

where θ is the angular coordinate defining the cylindrical polar base vectors

$$\begin{aligned}\boldsymbol{e}_r(\theta) &= \cos\theta\,\boldsymbol{e}_1 + \sin\theta\,\boldsymbol{e}_2,\\ \boldsymbol{e}_\theta(\theta) &= -\sin\theta\,\boldsymbol{e}_1 + \cos\theta\,\boldsymbol{e}_2,\\ \boldsymbol{e}_z &= \boldsymbol{e}_3,\end{aligned}$$

ω characterizes the angular velocity of the blade, and the functions $\{r, z, \phi_r, \phi_z\}$ of Z need to be determined.

Using these expressions it can be shown that

$$\begin{aligned}
\boldsymbol{F} &= \boldsymbol{d}_i \otimes \boldsymbol{D}^i = \Big(\frac{r}{R}\boldsymbol{e}_\theta\Big)\otimes\boldsymbol{e}_2 + \Big(\frac{dr}{dZ}\boldsymbol{e}_r + \frac{dz}{dZ}\boldsymbol{e}_z\Big)\otimes\boldsymbol{e}_z + (\phi_r\boldsymbol{e}_r + \phi_z\boldsymbol{e}_z)\otimes\boldsymbol{e}_1,\\
\boldsymbol{E}\cdot\boldsymbol{I} &= \frac{1}{2}\Big(\phi_r^2 + \phi_z^2 + \big(\frac{r}{R}\big)^2 + \big(\frac{dr}{dZ}\big)^2 + \big(\frac{dz}{dZ}\big)^2 - 3\Big),\\
\boldsymbol{\beta}_1 &= \Big(\frac{\phi_r}{r}\Big)\boldsymbol{e}_2, \qquad \boldsymbol{\beta}_2 = \frac{\big(\frac{d\phi_r}{dZ}\frac{dz}{dZ} - \frac{d\phi_z}{dZ}\frac{dr}{dZ}\big)\boldsymbol{e}_1 + \big(-\frac{d\phi_r}{dZ}\phi_z + \frac{d\phi_z}{dZ}\phi_r\big)\boldsymbol{e}_z}{\big(\frac{dz}{dZ}\phi_r - \frac{dr}{dZ}\phi_z\big)},\\
\boldsymbol{m}^1 &= \frac{H^3\mu^*}{12}\Bigg(\Big(\frac{2}{1-\nu^*}\Big)\Big(\frac{\phi_r}{r}\Big) + \big(\frac{2\nu^*}{1-\nu^*}\big)\frac{\big(-\frac{d\phi_r}{dZ}\phi_z + \frac{d\phi_z}{dZ}\phi_r\big)}{\big(\frac{dz}{dZ}\phi_r - \frac{dr}{dZ}\phi_z\big)}\Bigg)\frac{R}{r}\boldsymbol{e}_\theta,\\
\boldsymbol{m}^2 &= \frac{H^3\mu^*}{12}\Bigg(\Big(\frac{2\nu^*}{1-\nu^*}\Big)\Big(\frac{\phi_r}{r}\Big) + \Big(\frac{2}{1-\nu^*}\Big)\frac{\big(-\frac{d\phi_r}{dZ}\phi_z + \frac{d\phi_z}{dZ}\phi_r\big)}{\big(\frac{dz}{dZ}\phi_r - \frac{dr}{dZ}\phi_z\big)}\Bigg)\frac{(-\phi_z\boldsymbol{e}_r + \phi_r\boldsymbol{e}_z)}{(\frac{dz}{dZ}\phi_r - \frac{dr}{dZ}\phi_z)},\\
\boldsymbol{t}^1 &= \mu^* H\Bigg(\Big(\frac{2\nu^*}{1-2\nu^*}\Big)(\boldsymbol{E}\cdot\boldsymbol{I}) + \big(\frac{r}{R}\big)^2 - 1\Bigg)\frac{r}{R}\boldsymbol{e}_\theta - \frac{\phi_r}{r}\boldsymbol{m}^1,\\
\boldsymbol{t}^2 &= \mu^* H\Big(\big(\frac{2\nu^*}{1-2\nu^*}\big)(\boldsymbol{E}\cdot\boldsymbol{I})\Big)\Big(\frac{dr}{dZ}\boldsymbol{e}_r + \frac{dz}{dZ}\boldsymbol{e}_z\Big) + \mu^* H\Bigg(\Big(\frac{dr}{dZ}\phi_r + \frac{dz}{dZ}\phi_z\Big)(\phi_r\boldsymbol{e}_r + \phi_z\boldsymbol{e}_z)\\
&\qquad + \Bigg(\Big(\frac{dr}{dZ}\Big)^2 + \Big(\frac{dz}{dZ}\Big)^2 - 1\Bigg)\Big(\frac{dr}{dZ}\boldsymbol{e}_r + \frac{dz}{dZ}\boldsymbol{e}_z\Big)\Bigg) - \frac{(-\phi_z\frac{d\phi_r}{dZ} + \phi_r\frac{d\phi_z}{dZ})}{(\frac{dz}{dZ}\phi_r - \frac{dr}{dZ}\phi_z)}\boldsymbol{m}^2,\\
\boldsymbol{t}^3 &= \mu^* H\Bigg(\Big(\frac{2\nu^*}{1-2\nu^*}\Big)(\boldsymbol{E}\cdot\boldsymbol{I})\Bigg)(\phi_r\boldsymbol{e}_r + \phi_z\boldsymbol{e}_z)\\
&\quad + \mu^* H\Bigg(\big(\phi_r^2 + \phi_z^2 - 1\big)(\phi_r\boldsymbol{e}_r + \phi_z\boldsymbol{e}_z)\\
&\qquad + \Big(\phi_r\frac{dr}{dZ} + \phi_z\frac{dz}{dZ}\Big)\Big(\frac{dr}{dZ}\boldsymbol{e}_r + \frac{dz}{dZ}\boldsymbol{e}_z\Big)\Bigg) - \frac{(\frac{dz}{dZ}\frac{d\phi_r}{dZ} - \frac{dr}{dZ}\frac{d\phi_z}{dZ})}{(\frac{dz}{dZ}\phi_r - \frac{dr}{dZ}\phi_z)} - \boldsymbol{m}^2,\\
m\boldsymbol{b} &= q\Big(\frac{r}{R} - \frac{H}{2}\frac{\phi_r}{R}\Big)\Big(\Big(\frac{dz}{dZ} - \frac{H}{2}\frac{d\phi_z}{dZ}\Big)\boldsymbol{e}_r - \Big(\frac{dr}{dZ} - \frac{H}{2}\frac{d\phi_r}{dZ}\Big)\boldsymbol{e}_z\Big),\\
m\boldsymbol{b}^3 &= -\frac{qH}{2}\Big(\frac{r}{R} - \frac{H}{2}\frac{\phi_r}{R}\Big)\Big(\frac{dz}{dZ} - \frac{H}{2}\frac{d\phi_z}{dZ}\Big)\boldsymbol{e}_r\\
&\quad + \frac{qH}{2}\Big(\frac{r}{R} - \frac{H}{2}\frac{\phi_r}{R}\Big)\Big(\frac{dr}{dZ} - \frac{H}{2}\frac{d\phi_r}{dZ}\Big)\boldsymbol{e}_z + f_r(Z)\boldsymbol{e}_r,
\end{aligned} \tag{2–3}$$

where $\boldsymbol{t}^\alpha$ are forces and $\boldsymbol{m}^\alpha$ are couples, both measured per unit of deformed length of the blade's edges.

3. A simple finite deformation solution

In this section a simple solution is obtained where the plate is finitely deformed into a right-circular cylindrical shell and the effect of tensioning is neglected, that is, [$f_r = 0$ in (2–3)]. Specifically, for this solution the functions $\{r, z, \phi_r, \phi_z\}$ are

$$\begin{aligned} r &= c_1 R, \\ z &= c_2 Z, \\ \phi_r &= c_3, \\ \phi_z &= 0, \end{aligned} \tag{3–1}$$

where $\{c_1, c_2, c_3\}$ are constants. Now, substituting these functions into the expressions in (2–3), it can be shown that

$$\begin{aligned} \boldsymbol{m}^1 &= \frac{\mu^* H^3}{6(1-\nu^*)}\left(\frac{c_3}{c_1^2}\right)\frac{1}{R}\,\boldsymbol{e}_\theta, \\ \boldsymbol{m}^2 &= \frac{\mu^* H^3 \nu^*}{6(1-\nu^*)}\left(\frac{c_3}{c_1 c_2}\right)\frac{1}{R}\,\boldsymbol{e}_z, \\ \boldsymbol{t}^1 &= \mu^* H\left(\left(\frac{\nu^*}{1-2\nu^*}\right)(c_1^2+c_2^2+c_3^2-3)+(c_2^2-1)\right)c_1\boldsymbol{e}_\theta - \frac{\mu^* H^3}{6(1-\nu^*)}\left(\frac{c_3^2}{c_1^3}\right)\frac{H^2}{R^2}\boldsymbol{e}_\theta, \\ \boldsymbol{t}^2 &= \mu^* H\left(\left(\frac{\nu^*}{1-2\nu^*}\right)(c_1^2+c_2^2+c_3^2-3)+(c_2^2-1)\right)c_2\boldsymbol{e}_z, \\ \boldsymbol{t}^3 &= \mu^* H\left(\left(\frac{\nu^*}{1-2\nu^*}\right)(c_1^2+c_2^2+c_3^2-3)+(c_3^2-1)\right)c_3\boldsymbol{e}_r. \end{aligned}$$

Moreover, in the absence of contact stress q, the equations of motion (2–1) reduce to

$$\begin{aligned} \left(\left(\frac{\nu^*}{1-2\nu^*}\right)(c_1^2+c_2^2+c_3^2-3)+(c_1^2-1)\right) - \frac{1}{6(1-\nu^*)}\left(\frac{c_3^2}{c_1^4}\right)\frac{H^2}{R^2} &= \frac{\rho_0^* R^2\omega^2}{\mu^*}, \\ \left(\left(\frac{\nu^*}{1-2\nu^*}\right)(c_1^2+c_2^2+c_3^2-3)+(c_3^2-1)\right) + \frac{1}{6(1-\nu^*)}\left(\frac{1}{c_1^2}\right)\frac{H^2}{R^2} &= \frac{\rho_0^* H^2\omega^2}{\mu^*\pi^2}. \end{aligned} \tag{3–2}$$

In addition, for this solution it is assumed that the edges $Z = \pm W/2$ are free of resultant force ($\boldsymbol{t}^2 = 0$) so that

$$\left(\frac{\nu^*}{1-2\nu^*}\right)\left(c_1^2+c_2^2+c_3^2-3\right)+(c_2^2-1) = 0. \tag{3–3}$$

Next, by introducing the auxiliary constants

$$\begin{aligned} B_1 &= \frac{\nu^*}{1-\nu^*}, \\ B_2 &= \frac{1}{6(1-\nu^*)}\frac{H^2}{R^2}, \end{aligned}$$

the solution of (3–2) and (3–3) is obtained by solving the equation

$$(2B_1+1)c_1^8-\left((2B_1+1)+\frac{\rho_0^*R^2\omega^2(B_1+1)}{\mu^*}-B_1\frac{\rho_0^*H^2\omega^2}{\mu^*\pi^2}\right)c_1^6 \\ -\left(B_2(2B_1+1)+B_2\frac{\rho_0^*H^2\omega^2}{\mu^*\pi^2}\right)c_1^2+B_2^2=0,$$

for the positive real root of c_1 near unity, and substituting the solution into the equations

$$c_3^2-1=-\left(\frac{B_1}{B_1+1}\right)(c_1^2-1)-\left(\frac{B_2}{B_1+1}\right)\left(\frac{1}{c_1^2}\right)+\left(\frac{1}{B_1+1}\right)\frac{\rho_0^*H^2\omega^2}{\mu^*\pi^2},$$
$$c_2^2-1=-B_1\big(c_1^2+c_3^2-2\big),$$

for positive real values of $\{c_3, c_2\}$ near unity. In particular, note that since the value of $\boldsymbol{m}^2$ is nonzero it is necessary to specify a moment on the edges $Z=\pm W/2$ to maintain the right circular cylindrical shape of the deformed plate.

4. Linearized equations

To develop simplified equations for determining the contact stress between a deformed saw blade and the wheel, nonlinear equations associated with the kinematic assumption (2–2) are linearized about the finite deformation solution (3–1). Also, the function f_r associated with tensioning is assumed to be small. For these linearized equations the kinematics of the steady state deformations are specified by

$$r=c_1R+u_r(Z),$$
$$z=c_2Z+u_z(Z),$$
$$\phi_r=c_3+\delta_r(Z),$$
$$\phi_z=\delta_z(Z),$$

and quadratic terms in the displacements and the contact stress $\{u_r, u_z, \delta_r, \delta_z, q\}$ are neglected.

Straightforward algebraic manipulations yield expressions for the constitutive equations

$$\boldsymbol{t}^1=t_\theta^1\boldsymbol{e}_\theta$$
$$=\mu^*H\left(\left((c_1^2-c_2^2)c_1-\frac{c_3^2}{6(1-\nu^*)c_1^3}\frac{H^2}{R^2}\right)+\left((c_1^2-c_2^2)+\frac{2(1-\nu^*)}{(1-2\nu^*)}c_1^2+\frac{c_3^2}{2(1-\nu^*)c_1^4}\frac{H^2}{R^2}\right)\frac{u_r}{R}\right.$$
$$\left.+\left(\frac{2\nu^*c_1c_3}{(1-2\nu^*)}-\frac{c_3}{3(1-\nu^*)c_1^3}\frac{H^2}{R^2}\right)\delta_r+\left(\frac{2\nu^*c_1c_2}{1-2\nu^*}\right)\frac{du_z}{dZ}-\left(\frac{\nu^*c_3}{6(1-\nu^*)c_1^2c_2}\frac{H}{R}\right)H\frac{d\delta_z}{dZ}\right)\boldsymbol{e}_\theta,$$

$$
\begin{aligned}
\boldsymbol{t}^2 &= t_r^2\boldsymbol{e}_r + t_z^2\boldsymbol{e}_z = \mu^* H\Big(c_2c_3\delta_z + c_3^2\frac{du_r}{dZ}\Big)\boldsymbol{e}_r \\
&+2\mu^* H\Bigg(\Big(\frac{\nu^* c_1c_2}{1-2\nu^*}\Big)\frac{u_r}{R} + \Big(\frac{\nu^* c_2c_3}{1-2\nu^*}\Big)\delta_r + \Big(\frac{(1-\nu^*)c_2^2}{1-2\nu^*}\Big)\frac{du_z}{dZ} - \Big(\frac{\nu^* c_3}{12(1-\nu^*)c_1c_2^2}\frac{H}{R}\Big)H\frac{d\delta_z}{dZ}\Bigg)\boldsymbol{e}_z, \\
\boldsymbol{t}^3 &= t_r^3\boldsymbol{e}_r + t_z^3\boldsymbol{e}_z = \mu^* H\Bigg(\big(c_3^2-c_2^2\big)c_3 + \Big(\frac{2\nu^* c_1c_3}{1-2\nu^*}\Big)\frac{u_r}{R} + \Big(\big(c_3^2-c_2^2\big) + \frac{2(1-\nu^*)c_3^2}{1-2\nu^*}\Big)\delta_r \\
&\qquad + \Big(\frac{2\nu^* c_2c_3}{1-2\nu^*}\Big)\frac{du_z}{dZ}\Bigg)\boldsymbol{e}_r + \mu^* H\Bigg((c_3^2)\delta_z + (c_2c_3)\frac{du_r}{dZ} - \Big(\frac{\nu^*}{6(1-\nu^*)c_1c_2}\frac{H}{R}\Big)H\frac{d\delta_r}{dZ}\Bigg)\boldsymbol{e}_z, \\
\boldsymbol{m}^1 &= m_\theta^1\boldsymbol{e}_\theta = \mu^* H^2\Bigg(\Big(\frac{c_3}{6(1-\nu^*)c_1^2}\frac{H}{R}\Big) - \Big(\frac{c_3}{3(1-\nu^*)c_1^3}\frac{H}{R}\Big)\frac{u_r}{R} \\
&\qquad + \Big(\frac{1}{6(1-\nu^*)c_1^2}\frac{H}{R}\Big)\delta_r + \Big(\frac{\nu^*}{6(1-\nu^*)c_1c_2}\Big)H\frac{d\delta_z}{dZ}\Bigg)\boldsymbol{e}_\theta, \\
\boldsymbol{m}^2 &= m_r^2\boldsymbol{e}_r + m_z^2\boldsymbol{e}_z = \mu^* H^2\Bigg(-\Big(\frac{\nu^*}{6(1-\nu^*)c_1c_2}\frac{H}{R}\Big)\delta_z\Bigg)\boldsymbol{e}_r \\
&\qquad + \mu^* H^2\Bigg(\Big(\frac{\nu^* c_3}{6(1-\nu^*)c_1c_2}\frac{H}{R}\Big) - \Big(\frac{\nu^* c_3}{6(1-\nu^*)c_1^2c_2}\frac{H}{R}\Big)\frac{u_r}{R} \\
&\qquad + \Big(\frac{\nu^*}{6(1-\nu^*)c_1c_2}\frac{H}{R}\Big)\delta_r - \Big(\frac{\nu^* c_3}{6(1-\nu^*)c_1c_2^2}\frac{H}{R}\Big)\frac{du_z}{dZ} + \Big(\frac{1}{6(1-\nu^*)c_2^2}\Big)H\frac{d\delta_z}{dZ}\Bigg)\boldsymbol{e}_z, \\
m\boldsymbol{b} &= q\Big(c_1c_2 - \frac{c_2c_3H}{2R}\Big)\boldsymbol{e}_r, \\
m\boldsymbol{b}^3 &= -qH\Big(\frac{c_1c_2}{2} - \frac{c_2c_3}{4}\frac{H}{R}\Big)\boldsymbol{e}_r + f_r\boldsymbol{e}_r.
\end{aligned}
\tag{4–1}
$$

Then, the linearized equations of motion for the steady state deformations become

$$
\begin{aligned}
0 &= q\Big(c_1c_2 - \frac{c_2c_3H}{2R}\Big) \\
&\quad + \mu^*\Bigg(\Big(-\big(c_1^2-c_2^2\big)\frac{H}{R} - \frac{2(1-\nu^*)c_1^2}{1-2\nu^*}\frac{H}{R} - \frac{c_3^2}{2(1-\nu^*)c_1^4}\frac{H^3}{R^3} + \frac{\rho_0^* HR\omega^2}{\mu^*}\Big)\frac{u_r}{R} \\
&\qquad + \Big(-\frac{2\nu^* c_1c_3}{1-2\nu^*}\frac{H}{R} + \frac{c_3}{3(1-\nu^*)c_1^3}\frac{H^3}{R^3}\Big)\delta_r - \Big(\frac{2\nu^* c_1c_2}{1-2\nu^*}\frac{H}{R}\Big)\frac{du_z}{dZ} \\
&\qquad\quad + \Big(c_2c_3 + \frac{\nu^* c_3}{6(1-\nu^*)c_1^2c_2}\frac{H^2}{R^2}\Big)H\frac{d\delta_z}{dZ} + (c_3^2)H\frac{d^2u_r}{dZ^2}\Bigg),
\end{aligned}
\tag{4–2a}
$$

$$0=\frac{d}{dZ}\Big(\Big(\frac{\nu^* c_1c_2}{1-2\nu^*}\Big)\frac{u_r}{R}+\Big(\frac{\nu^* c_2c_3}{1-2\nu^*}\Big)\delta_r+\Big(\frac{(1-\nu^*)c_2^2}{1-2\nu^*}\Big)\frac{du_z}{dZ} - \Big(\frac{\nu^* c_3}{12(1-\nu^*)c_1c_2^2}\frac{H}{R}\Big)H\frac{d\delta_z}{dZ}\Big), \tag{4–2b}$$

$$\begin{aligned}0=&-q\Big(\frac{c_1c_2}{2}-\frac{c_2c_3}{4}\frac{H}{R}\Big)\\&+\mu^*\Big(\Big(-\frac{2\nu^* c_1c_3}{1-2\nu^*}+\frac{c_3}{3(1-\nu^*)c_1^3}\frac{H^2}{R^2}\Big)\frac{u_r}{R}\\&\quad+\Big(-(c_3^2-c_2^2)-\frac{2(1-\nu^*)c_3^2}{1-2\nu^*}-\frac{1}{6(1-\nu^*)c_1^2}\frac{H^2}{R^2}+\frac{\rho_0^* H^2\omega^2}{\mu^*\pi^2}\Big)\delta_r\\&\qquad-\Big(\frac{2\nu^* c_2c_3}{1-2\nu^*}\Big)\frac{du_z}{dZ}-\Big(\frac{\nu^*}{3(1-\nu^*)c_1c_2}\frac{H}{R}\Big)H\frac{d\delta_z}{dZ}\Big)+f_r,\end{aligned} \tag{4–2c}$$

$$\begin{aligned}0=&-(c_3^2)\delta_z+\Big(-c_2c_3-\frac{\nu^* c_3}{6(1-\nu^*)c_1^2c_2}\frac{H^2}{R^2}\Big)\frac{du_r}{dZ}\\&+\Big(\frac{\nu^*}{3(1-\nu^*)c_1c_2}\frac{H}{R}\Big)H\frac{d\delta_r}{dZ}-\Big(\frac{\nu^* c_3}{6(1-\nu^*)c_1c_2^2}\frac{H}{R}\Big)H\frac{d^2u_z}{dZ^2}\\&+\Big(\frac{1}{6(1-\nu^*)c_2^2}\Big)H^2\frac{d^2\delta_z}{dZ^2}.\end{aligned} \tag{4–2d}$$

Moreover, the radial gap Δ of blade's inner surface relative to the radius of the wheel is defined by

$$\Delta=\Big(c_1R-\frac{H}{2}c_3\Big)+\Big(u_r-\frac{H}{2}\delta_r\Big)-R_W. \tag{4–3}$$

The effects of tensioning on the stiffness and frequencies of vibration of the blade have been studied by [Lister and Schajer 1993] using a model based on deformations of a plate. The linearized equations (4–2a)–(4–2d) and (4–3) can be used to determine the influence of both tensioning and different crowned shapes of the wheel on contact stress q by specifying forms for the tensioning function $f_r(Z)$ and the wheel radius $R_W(Z)$. For the general case, portions of the blade are in contact with the wheel and other portions are free of contact. For a specified form of the tensioning function $f_r(Z)$ the equations (4–2) are solved for $\{u_r, u_z, \delta_r, \delta_z\}$ with $q=0$ in the free regions. In contact regions Δ, as defined in (4–3) vanishes and the equations (4–2) and (4–3) are solved for $\{u_r, u_z, \delta_r, \delta_z, q\}$. Consequently, the tensioning function f_r influences the functional form of the radial displacement u_r which in turn controls the shape of the blade in free regions and influences the contact stress q in contact regions.

Here, the effects of tensioning and the crowned shape of the wheel are omitted by specifying $f_r=0$ and a constant value for R_W and attention is focused on assessing the influence of elastic deformations caused by bending a plate into a circular cylindrical shell. Specifically, the wheel is taken to have a

uniform radius, with the blade and wheel specified by

$$E^* = 200\,\text{GPa}, \qquad \mu^* = \frac{E^*}{2(1+\nu^*)}, \qquad \nu^* = 0.3,$$
$$\rho_0^* = 7.85\,\text{Mg/m}^3, \qquad H = 0.0016\,\text{m}, \qquad W = 0.20\,\text{m}, \qquad R_W = 0.8\,\text{m}. \tag{4–4}$$

These values are typical dimensions for wide saw blades used in industrial wood cutting band saws. For other possible values see [Lister and Schajer 1993; Chung and Sung 1998; Damaren and Le-Ngoc 2000]. Using a normalized axial coordinate

$$\alpha = \frac{Z}{W}, \tag{4–5}$$

the wheel's edge is specified by

$$\alpha = \alpha_W = 0.4, \tag{4–6}$$

indicating that 10% of the blade hangs over the wheel's edge (Figure 1). The portion of the blade weakened by the gullets which form the blade's teeth is assumed to provide negligible strength. Also, the reference length of the blade is specified by the normalized misfit of the blade η defined so that

$$R - \frac{H}{2} = R_W + \eta H. \tag{4–7}$$

This formula treats the deformed blade as a right circular cylindrical shell with an inner radius larger than the wheel's radius by the amount of ηH.

Details of the solution will be presented in the next section. However, here qualitative aspects are presented in order to discuss the nature of the boundary conditions. Specifically, attention is focused on the following three cases:

Case 1: $\omega = 0$; $\eta \geq \eta_1$: 1 free region

Free region: $-0.5 \leq \alpha \leq 0.5$,

Case 2: $\omega = 0$; $\eta_3 \leq \eta \leq \eta_2$: 2 free regions and 1 contact region with $\alpha_2 < \alpha_W$

Free regions: $-0.5 \leq \alpha \leq \alpha_1$, $\qquad \alpha_2 \leq \alpha \leq 0.5$,

Contact region: $\alpha_1 \leq \alpha \leq \alpha_2 < \alpha_W$,

Case 3: $\omega = 0$; $\eta \leq \eta_3$: 2 free regions and 1 contact region with $\alpha_2 = \alpha_W$

Free regions: $-0.5 \leq \alpha \leq \alpha_1$, $\qquad \alpha_2 = \alpha_W \leq \alpha \leq 0.5$,

Contact region: $\alpha_1 \leq \alpha \leq \alpha_W$.

The cases are characterized by three values of η

$$\eta_3 < \eta_2 < \eta_1,$$

and two values of α

$$-0.5 < \alpha_1 < \alpha_2 \leq \alpha_W < 0.5.$$

For Case 1 the blade is free and contact first begins at the two points $\alpha = \alpha_1$ and $\alpha = \alpha_2 = -\alpha_1$ when $\eta = \eta_1$. For η between the values η_1 and η_2, the solution is characterized by multiple free and contact regions.

The solutions in this range of η are complicated and are not particularly significant from an engineering point of view since the contact stresses remain quite low. Therefore, they will not be analyzed in this paper. When $\eta = \eta_2$ these complications disappear and the solution is characterized by Case 2 with two free regions and one contact region $\alpha_1 \le \alpha \le \alpha_2 = -\alpha_1$ and with the blade separating from the wheel before it reaches the wheel's edge ($\alpha_2 < \alpha_W$). Case 3 is also characterized by two free regions and one contact region which now extends to the wheel's edge ($\alpha_2 = \alpha_W$).

In the context of the present theory it is possible to specify three boundary conditions at each edge. It can be seen from (4–1) that the equation of motion (4–2b) requires the axial component of force per unit length to be constant

$$t_z^2 = \text{constant}\,. \tag{4–8}$$

The boundary conditions at the edges $\alpha = \pm 0.5$ and the continuity conditions at the boundaries of the free and contact regions are specified by

$$t_r^2 = 0, \tag{4–9a}$$

$$t_z^2 = 0, \tag{4–9b}$$

$$m_z^2 = 0, \quad \text{for } \alpha = -0.5, \tag{4–9c}$$

$$\left\{u_r, u_z, \delta_r, \delta_z, t_r^2, t_z^2\right\} \text{ are continuous for } \alpha = \alpha_i \ (i = 1, 2), \tag{4–9d}$$

$$u_z = 0, \qquad \text{for } \alpha = \alpha_W, \tag{4–9e}$$

$$t_r^2 = 0, \quad m_z^2 = 0, \qquad \text{for } \alpha = 0.5. \tag{4–9f}$$

Here, $\{t_r^2, t_z^2, m_r^2, m_z^2\}$ correspond, respectively, to the shear force, the axial force, a pinching moment, and a bending moment, each measured per unit length of the blade's edge. The conditions (4–9a), (4–9b), (4–9c), (4–9f) together with the result (4–8) indicate that the edges $\alpha = \pm 0.5$ are nearly traction free. The theory is not general enough to ensure that the pinching moment m_r^2 vanishes at these edges or that it is continuous at the boundaries (α_1, α_2). Also, (4–9d) requires continuity of the normal strain δ_r instead of continuity of the bending moment m_z^2. This means that the geometry of the blade will be continuous at the boundaries (α_1, α_2) but that the moments $\{m_r^2, m_z^2\}$ can experience jumps there. Furthermore, the condition (4–9e) removes rigid body translation and requires the same material point on the blade to remain at the wheel's edge.

The locations (α_1, α_2) of the boundaries of the contact regions are determined by the condition that the contact stress q in the contact region vanishes at these boundaries and that it is positive in the interior of the contact region. Therefore, this condition requires

$$\text{Case 2: } q = 0, \quad \text{for } \alpha = \alpha_1, \alpha_2, \tag{4–10a}$$

$$\text{Case 3: } q = 0, \quad \text{for } \alpha = \alpha_1. \tag{4–10b}$$

In particular, in Case 3 the contact stress at the wheel's edge ($\alpha = \alpha_W$) can suddenly decrease from a positive value in the contact region to zero in the free region. Also, to discuss the results presented below

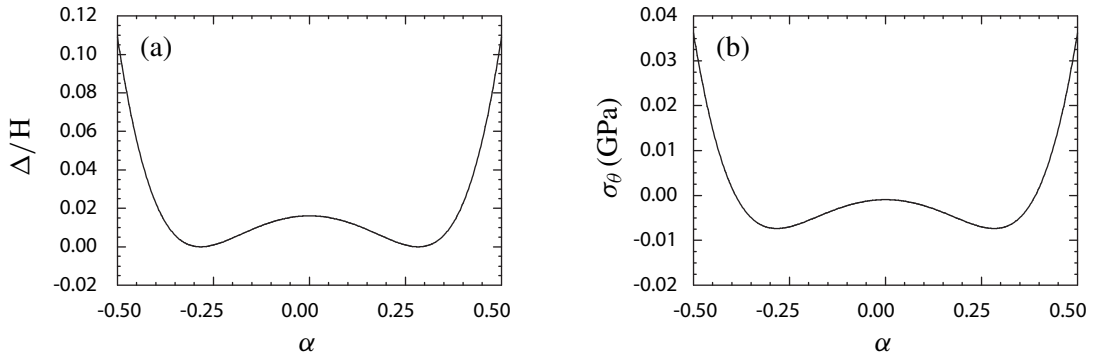

Figure 2. Plots of the radial gap Δ normalized by the thickness H and the circumferential stress σ_θ as functions of the normalized axial coordinate α for the onset of contact with the normalized misfit of the blade $\eta = \eta_1$ and no angular velocity $\omega = 0$.

it is convenient to approximate the Cauchy circumferential stress σ_θ in the band saw blade as

$$\sigma_\theta = \frac{t_\theta^1}{c_3 H}, \tag{4–11}$$

where t_θ^1 is the force per unit present length, and $c_3 H$ is the present thickness.

Using the solution we present in the following section, we can show that

$$\eta_1 = 1.8171E-2, \qquad \eta_2 = -2.6268E-04, \qquad \eta_3 = -1.4676E-1 \quad \text{for } \omega = 0. \tag{4–12}$$

Figure 2 shows results for Case 1 with $\eta = \eta_1$ and $\omega = 0$ which causes the blade to just make contact with the wheel. Figure 2a shows the deformed inner surface of the blade Δ (4–3) and Figure 2b shows the circumferential stress σ_θ, both as functions of the normalized axial coordinate α. In Figure 2a note that the edges $\alpha = \pm 0.5$ experience localized bending due to the relief of the edge moments that must be applied to the simple solution of Section 3. In Figure 2b note that the circumferential stress has a shape similar to the radial gap Δ in Figure 2a, with the center region being compressive (negative values) and the edges being tensile (positive values).

5. Solution procedure

In view of the conditions (4–8), (4–9b),and (4–9d), the expression for t_z^2 in (4–1) can be solved for δ_r in both the free and contact regions to obtain

$$\delta_r = -\Big(\frac{c_1}{c_3}\Big)\frac{u_r}{R} - \Big(\frac{(1-\nu^*)c_2}{\nu^* c_3}\Big)\frac{du_z}{dZ} + \Big(\frac{(1-2\nu^*)}{12(1-\nu^*)c_1 c_2^3}\frac{H}{R}\Big)H\frac{d\delta_z}{dZ}. \tag{5–1}$$

Equation (4–2c) for the contact stress can now be rewritten as

$$q\Big(c_1c_2-\frac{c_2c_3H}{2R}\Big)=\mu^*\Bigg(\Big(4c_1c_3+\frac{2c_1(c_3^2-c_2^2)}{c_3}+\frac{(c_1^2+2c_3^2)}{3(1-\nu^*)c_1^3c_3}\frac{H^2}{R^2}-\frac{2\rho_0^*H^2\omega^2c_1}{\mu^*\pi^2c_3}\Big)\frac{u_r}{R}$$
$$+\Big(\frac{4c_2c_3}{\nu^*}+\frac{2(1-\nu^*)(c_3^2-c_2^2)c_2}{\nu^*c_3}+\frac{c_2}{3\nu^*c_1^2c_3}\frac{H^2}{R^2}-\frac{2\rho_0^*H^2\omega^2(1-\nu^*)c_2}{\mu^*\pi^2\nu^*c_3}\Big)\frac{du_z}{dZ}$$
$$+\Big(-\frac{2\nu^*}{3(1-\nu^*)c_1c_2}-\frac{(1-2\nu^*)(c_3^2-c_2^2)}{6(1-\nu^*)c_1c_2^3}-\frac{c_3^2}{3c_1c_2^3}$$
$$-\frac{(1-2\nu^*)}{36(1-\nu^*)^2c_1^3c_2^3}\frac{H^2}{R^2}+\frac{\rho_0^*H^2\omega^2(1-2\nu^*)}{6\mu^*\pi^2(1-\nu^*)c_1c_2^3}\Big)\frac{H^2}{R}\frac{d\delta_z}{dZ}\Bigg). \quad (5\text{–}2)$$

Next, using (5–1) and (5–2) the remaining equations of motion (4–2a), (4–2d) become

$$\Bigg(4c_1c_3+\frac{2c_1(c_3^2-c_2^2)}{c_3}-\big(3c_1^2-c_2^2\big)\frac{H}{R}+\frac{(c_1^2+2c_3^2)}{3(1-\nu^*)c_1^3c_3}\frac{H^2}{R^2}$$
$$-\frac{(2c_1^2+3c_3^2)}{6(1-\nu^*)c_1^4}\frac{H^3}{R^3}+\frac{\rho_0^*HR\omega^2}{\mu^*}-\frac{2\rho_0^*H^2\omega^2c_1}{\mu^*\pi^2c_3}\Big)\frac{u_r}{R}$$
$$+\Big(\frac{4c_2c_3}{\nu^*}+\frac{2(1-\nu^*)(c_3^2-c_2^2)c_2}{\nu^*c_3}+2c_1c_2\frac{H}{R}+\frac{c_2}{3\nu^*c_1^2c_3}\frac{H^2}{R^2}$$
$$-\frac{c_2}{3\nu^*c_1^3}\frac{H^3}{R^3}-\frac{2\rho_0^*H^2\omega^2(1-\nu^*)c_2}{\mu^*\pi^2\nu^*c_3}\Big)\frac{du_z}{dZ}$$
$$+\Big(c_2c_3-\frac{(6\nu^*-1)c_2^2+(3-4\nu^*)c_3^2}{6(1-\nu^*)c_1c_2^3}\frac{H}{R}+\frac{\nu^*c_3(c_2^2-c_1^2)}{6(1-\nu^*)c_1^2c_2^3}\frac{H^2}{R^2}$$
$$-\frac{(1-2\nu^*)}{36(1-\nu^*)^2c_1^3c_2^3}\frac{H^3}{R^3}+\frac{(1-2\nu^*)c_3}{36(1-\nu^*)^2c_1^4c_2^3}\frac{H^4}{R^4}+\frac{\rho_0^*H^2\omega^2(1-2\nu^*)}{6\mu^*\pi^2(1-\nu^*)c_1c_2^3}\frac{H}{R}\Big)H\frac{d\delta_z}{dZ}$$
$$+\{c_3^2\}H\frac{d^2u_r}{dZ^2}=0, \quad (5\text{–}3a)$$

$$\{c_3^2\}\delta_z+\Big(c_2c_3+\frac{\nu^*(2c_1^2+c_3^2)}{6(1-\nu^*)c_1^2c_2c_3}\frac{H^2}{R^2}\Big)\frac{du_r}{dZ}+\Big(\frac{\nu^*c_3}{6(1-\nu^*)c_1c_2^2}+\frac{1}{3c_1c_3}\Big)\frac{H^2}{R}\frac{d^2u_z}{dZ^2}$$
$$-\Big(\frac{1}{6(1-\nu^*)c_2^2}+\frac{\nu^*(1-2\nu^*)}{36(1-\nu^*)^2c_1^2c_2^4}\frac{H^2}{R^2}\Big)H^2\frac{d^2\delta_z}{dZ^2}=0. \quad (5\text{–}3b)$$

Now, for free regions the contact stress q vanishes and the equations of motion (5–2) and (5–3) can be rewritten as six first order equations in the matrix form

$$\sum_{j=1}^{6}\Big(A_{ij}^f\frac{dy_j^f}{dZ}+B_{ij}^fy_j^f\Big)=0, \quad (5\text{–}4)$$

in terms of the vector

$$y_i^f = \Big(u_r, u_z, \delta_z, \frac{du_r}{dZ}, \frac{du_z}{dZ}, \frac{d\delta_z}{dZ}\Big), \tag{5–5}$$

where the components of the $\{A_{ij}^f, B_{ij}^f\}$ are recorded in Appendix A. The characteristic equation for the eigenvalues λ associated with (5–4) becomes

$$\lambda\big(a_2^f \lambda^4 + a_1^f \lambda^2 + a_0^f\big) = 0, \tag{5–6}$$

where a_i^f are real constants given in (A–1). It then follows that (5–4) represents a fifth order system with eigenvalues that take the forms

$$\lambda = \pm\lambda_1^f, \pm\lambda_3^f, 0; \qquad \lambda_1^f = \big(\lambda_{R1}^f \pm i\lambda_{I1}^f\big), \qquad \lambda_3^f = \big(\lambda_{R3}^f \pm i\lambda_{I3}^f\big), \tag{5–7}$$

where $\{\lambda_{R1}^f, \lambda_{I1}^f, \lambda_{R3}^f, \lambda_{I3}^f\}$ are real positive numbers and $i = \sqrt{-1}$. The five independent eigenfunctions ϕ_j^f $(j = 1, 2, \ldots, 5)$ are, for $(-W/2 \le Z \le \alpha_1 W)$,

$$\begin{aligned}
\phi_1^f(Z) &= \mathrm{Re}\Big(Y_{1j}^f \exp\big(\lambda_1^f (Z-\beta)\big)\Big),\\
\phi_2^f(Z) &= \mathrm{Im}\Big(Y_{1j}^f \exp\big(\lambda_1^f (Z-\beta)\big)\Big),\\
\phi_3^f(Z) &= \mathrm{Re}\Big(Y_{3j}^f \exp\big(\lambda_3^f (Z-\beta)\big)\Big),\\
\phi_4^f(Z) &= \mathrm{Im}\Big(Y_{3j}^f \exp\big(\lambda_3^f (Z-\beta)\big)\Big),\\
\phi_5^f &= (0, 1, 0, 0, 0, 0),\\
\beta &= \tfrac{1}{2}\Big(-\tfrac{1}{2} + \alpha_1\Big)W \quad \text{for } -\tfrac{W}{2} \le Z \le \alpha_1 W,\\
\beta &= \tfrac{1}{2}\Big(\tfrac{1}{2} + \alpha_2\Big)W \quad \text{for } -\alpha_2 W \le Z \le \tfrac{W}{2},
\end{aligned} \tag{5–8}$$

where α_1 and α_2 represent the boundaries of the free region in consideration, β is the average of the these boundaries, $\mathrm{Re}(x)$ and $\mathrm{Im}(x)$ represent the real and imaginary parts of the complex quantity x, and $\{Y_{1j}^f, Y_{3j}^f\}$ are the eigenvectors which satisfy the equations

$$\sum_{j=1}^{6}\big(A_{ij}^f \lambda_1^f + B_{ij}^f\big)Y_{1j}^f = 0, \qquad \sum_{j=1}^{6}\big(A_{ij}^f \lambda_3^f + B_{ij}^f\big)Y_{3j}^f = 0. \tag{5–9}$$

Then, the solution in the free region takes the general form

$$y_i^f(Z) = \sum_{j=1}^{5} c_j^f \phi_j^f(Z), \tag{5–10}$$

where c_j^f are real constants to be determined by the boundary conditions. Moreover, for this solution δ_r is obtained by (5–1).

In the contact regions the value of δ_r in (5–1) is restricted so that Δ in (4–3) vanishes, which yields

$$\Big(1+\frac{c_1}{2c_3}\frac{H}{R}\Big)\frac{u_r}{R}+\Big(\frac{(1-\nu^*)c_2}{2\nu^* c_3}\Big)\frac{H}{R}\frac{du_z}{dZ}-\Big(\frac{(1-2\nu^*)}{24(1-\nu^*)c_1c_2^3}\Big)\frac{H^3}{R^2}\frac{d\delta_z}{dZ}=-\Big(c_1-\frac{H}{2R}c_3-\frac{R_W}{R}\Big). \quad (5–11)$$

For the contact regions the contact stress q in (5–2) is required to remain positive (except at the boundaries of the regions) and the equations of motion (5–11) and (5–3) can be rewritten as six first order equations in the matrix form

$$\sum_{j=1}^{6}\Big(A_{ij}^c\frac{dy_j^c}{dZ}+B_{ij}^c y_j^c\Big)=C_i^c, \quad (5–12)$$

in terms of the vector

$$y_i^c=\Big(u_r,u_z,\delta_z,\frac{du_r}{dZ},\frac{du_z}{dZ},\frac{d\delta_z}{dZ}\Big), \quad (5–13)$$

where the components of $\{A_{ij}^c, B_{ij}^c, C_i^c\}$ are given in Appendix A. The solution in the contact region is obtained in a manner similar to that in the free regions. Specifically, the characteristic equation for the eigenvalues λ associated with the homogeneous solution of (5–12) becomes

$$\lambda\big(a_2^c\lambda^4+a_1^c\lambda^2+a_0^c\big)=0, \quad (5–14)$$

where a_i^c are real constants given in (A–2). It then follows that (5–14) represents a fifth order system with eigenvalues that take the forms

$$\lambda=\pm\lambda_1^c,\pm\lambda_3^c,0; \qquad \lambda_1^c=\big(\lambda_{R1}^c\pm i\lambda_{I1}^c\big), \qquad \lambda_3^c=\big(\lambda_{R3}^c\pm i\lambda_{I3}^f\big), \quad (5–15)$$

where $\{\lambda_{R1}^f,\lambda_{I1}^f,\lambda_{R3}^f,\lambda_{I3}^f\}$ are real positive numbers. The five independent eigenfunctions

$$\phi_i^c\ (i=1,2,\ldots,5)$$

are specified in the forms

$$\phi_1^c(Z)=\mathrm{Re}\Big(Y_{1i}^c\exp\big(\lambda_1^c(Z-\beta)\big)\Big), \qquad \phi_2^c(Z)=\mathrm{Im}\Big(Y_{3i}^c\exp\big(\lambda_1^c(Z-\beta)\big)\Big), \quad (5–16)$$

$$\phi_3^c(Z)=\mathrm{Re}\Big(Y_{3i}^c\exp\big(\lambda_3^c(Z-\beta)\big)\Big), \qquad \phi_4^c(Z)=\mathrm{Im}\Big(Y_{3i}^c\exp\big(\lambda_3^c(Z-\beta)\big)\Big), \quad (5–17)$$

$$\phi_5^c=(0,1,0,0,0,0), \qquad \beta=\tfrac{1}{2}W\big(\alpha_1+\alpha_2\big), \quad (5–18)$$

where $\{Y_{1i}^c, Y_{3i}^c\}$ are the eigenvectors which satisfy the equations

$$\sum_{j=1}^{6}\big(A_{ij}^c\lambda_1^c+B_{ij}^c\big)Y_{1j}^c=0, \qquad \sum_{j=1}^{6}\big(A_{ij}^c\lambda_3^c+B_{ij}^c\big)Y_{3j}^c=0. \quad (5–19)$$

In addition, the equations (5–12) require a specific solution of the form

$$y_1^{cP}=\frac{B_{55}^cC_4^c}{B_{41}^cB_{55}^c-B_{45}^cB_{51}^c}, \qquad y_2^{cP}=-\left(\frac{B_{51}^cC_4^c}{B_{41}^cB_{55}^c-B_{45}^cB_{51}^c}\right)Z, \quad (5–20)$$

$$y_5^{cP}=-\left(\frac{B_{51}^cC_4^c}{B_{41}^cB_{55}^c-B_{45}^cB_{51}^c}\right), \qquad y_3^{cP}=y_4^{cP}=y_6^{cP}=0. \quad (5–21)$$

Then, the solution in the contact region takes the general form

$$y_i^c(Z) = \sum_{j=1}^{5} c_j^c \phi_j^f(Z) + y_i^{cP}(Z), \tag{5–22}$$

where c_j^c are real constants to be determined by the boundary conditions. Moreover, for this solution δ_r is obtained by (5–1) and the contact stress q is determined by (5–2).

The specification (5–1) for δ_r satisfies the condition that t_z^2 vanishes so that boundary conditions on t_z^2 in (4–9) are automatically satisfied. The solutions (5–10) and (5–22) show that there are five constants to be determined in each of the free and contact regions as well as the boundary values of α_i. For the three cases we present, unknowns and equations are given by:

Case 1:

Unknowns: 5 values of c_j^f;
Equations: (4–9a), (4–9c), (4–9e), (4–9f);

Case 2:

Unknowns: 10 values of c_j^f, 5 values of c_j^c, $\{\alpha_1, \alpha_2\}$;
Equations: (4–9a), (4–9c), 10 Equations (4–9d), (4–9e), (4–9f), 2 Equations (4–10a);

Case 3:

Unknowns: 10 values of c_j^f, 5 values of c_j^c, $\{\alpha_1\}$;
Equations: (4–9a), (4–9c), 10 Equations (4–9d), (4–9e), (4–9f), 1 Equation (4–10b).

6. Discussion

The equations of the previous section were solved for the problem characterized by (4–4) and (4–6). Figures 3 and 4 plot values of (a) the radial gap Δ (4–3), (b) the circumferential stress σ_θ (4–11), and (c) and (d) the contact stress q as functions of the normalized axial coordinate α in (4–5) for $\omega = 0$ and different values of misfit η (4–7). Specifically, Figure 3 shows the solution for Case 2 associated with the largest value of $\eta = \eta_2$ (4–12) for which the blade has a single contact region with the wheel and Figure 4 shows the solution for Case 3 associated with the largest value of $\eta = \eta_3$ (4–12) for which the blade has a single contact region that extends to the edge ($\alpha = \alpha_W$) of the wheel. Figure 5 shows plots of the following values: the radial gap Δ (Figure 5a,b); the circumferential stress σ_θ (Figure 5c); and the contact stress q (Figure 5d–f) for a high value of tension of $\eta = -2.5$ and $\omega = 0$. Also, these figures include the predictions of the Lamé solution discussed in Appendix B.

Figure 3a, b, Figure 4a, b and Figure 5a,c show that the plots of circumferential stress σ_θ have the same shapes as those of the radial gap Δ. This means that the circumferential tension is dominated by the radial displacement of the saw blade. Figure 5b shows that even for the case of high tension, the end of the blade near $\alpha = -0.5$ is separated from the wheel. Figures 3c and 4c show two spikes in the contact stress which occur near the regions where the free saw blade has the smallest radius, as shown in Figure 2. For Cases 2 and 3 the shape of the contact stress curve in these regions is symmetrical (Figure 3d and Figure 4d). As Figure 5d–f shows, when the tension is high enough to cause the edge $\alpha = \alpha_W$ to be in contact with the saw blade, the contact stress is no longer symmetrical with the maximum contact stress occurring near the edge $\alpha = \alpha_W$ of the wheel. In particular, the maximum contact stress near the

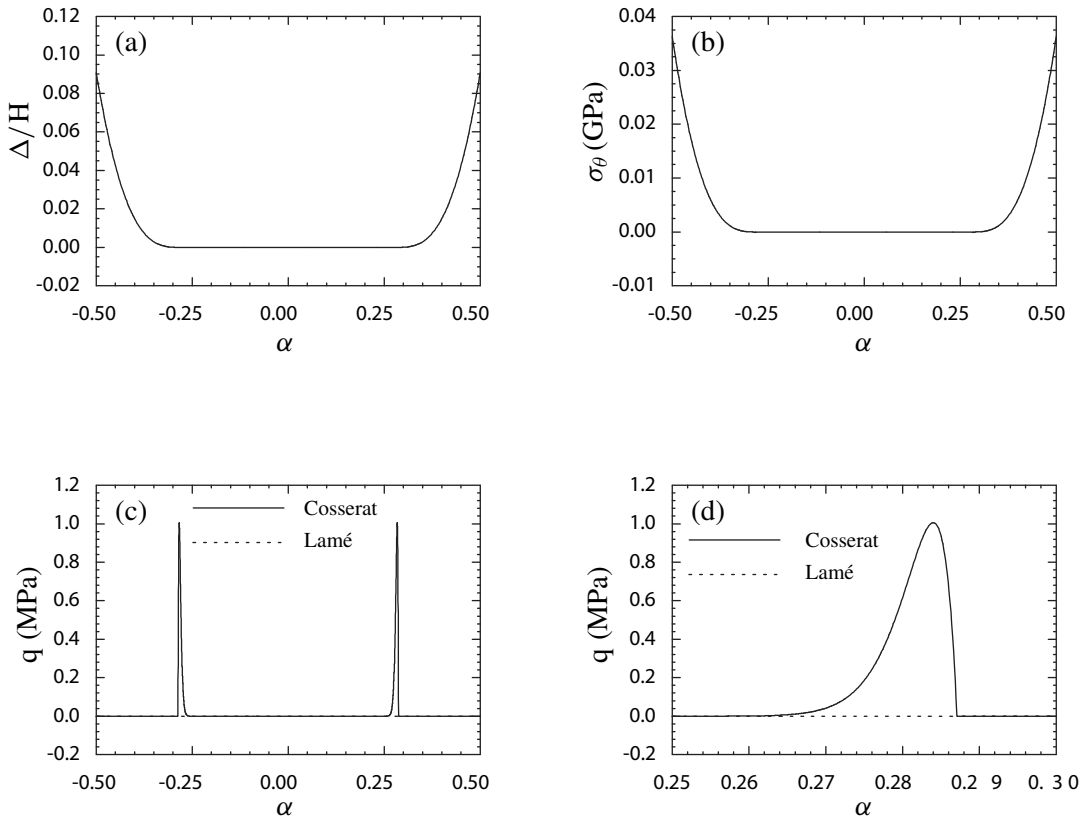

Figure 3. Plots of the radial gap Δ normalized by the thickness H, the circumferential stress σ_θ and the contact stress q as functions of the normalized axial coordinate α for the onset of a single contact region with the normalized misfit of the blade $\eta = \eta_2$ and no angular velocity $\omega = 0$.

edge $\alpha = \alpha_W$ is more than three times that near the edge $\alpha = \alpha_1$ for $\eta = -2.5$. Also, Figure 5f shows that the contact stress exhibits a small decrease from the value $q = 0.9$ MPa to zero at the edge $\alpha = \alpha_W$.

Moreover, from Figure 5d–f it can be seen that the Lamé solution predicts a uniform contact stress of about 2 MPa which significantly underpredicts the value of maximum contact stress as well as the value in the nearly uniform region in the center of the wheel. This means that for an accurate prediction of the contact stress it is essential to include an analysis of the nonlinear deformation associated with the formation of the saw blade from a flat plate. In practice, the tensioning process is used to change the deformed shape of the saw blade by applying controlled plastic deformations. Although the analysis of plastic deformations is outside of the scope of the present paper, the results presented here suggest that this process should be carefully analyzed since it could significantly affect the resulting distribution of contact stress.

The speed of a band saw is often measured in terms of its translational velocity. For example, a velocity of 2800 m/min is typical for an industrial wood cutting blade [Lunstrum 1981; 1984]. Also see

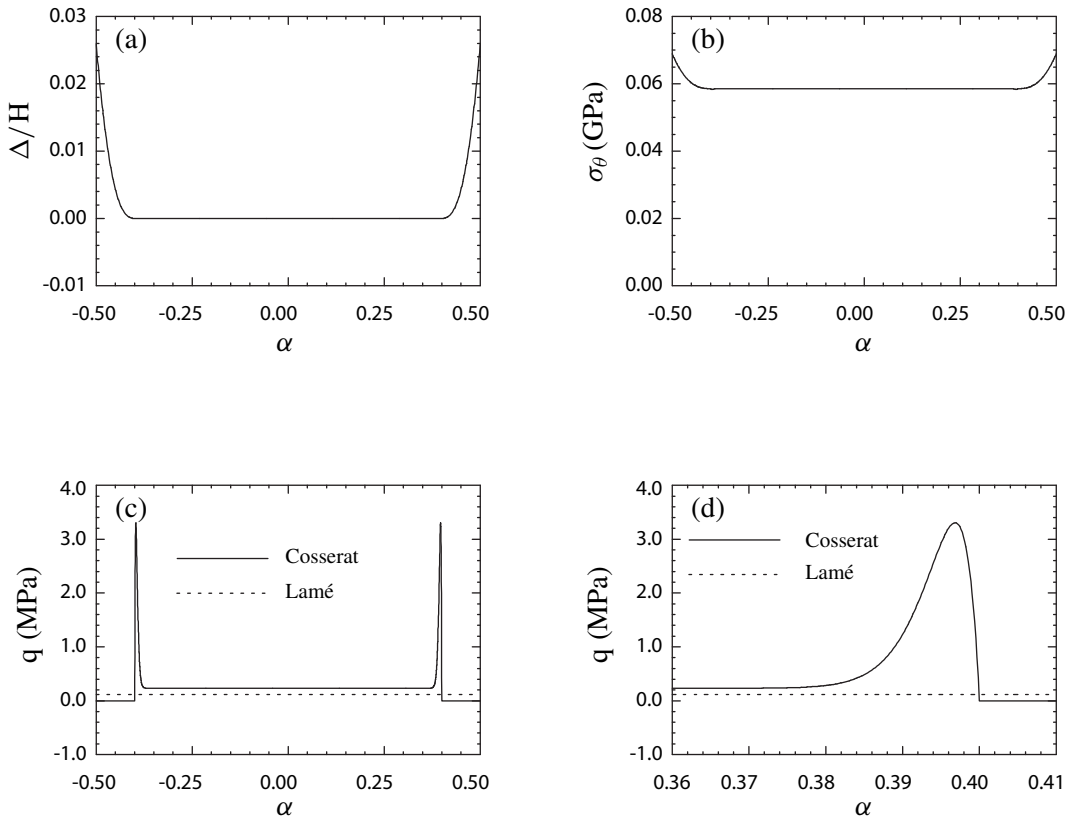

Figure 4. Plots of the radial gap Δ normalized by the thickness H, the circumferential stress σ_θ and the contact stress q as functions of the normalized axial coordinate α for the point at which a single contact region reaches the edge of the wheel with the normalized misfit of the blade $\eta = \eta_3$ and no angular velocity $\omega = 0$.

[Eklund 2000; Murata et al. 2002] for velocities associated with other saws. An estimate of the influence of rotation on the contact stress can be obtained by equating this translational velocity with the velocity v_W of the blade at the surface of the wheel

$$\omega = \frac{v_W}{R_W}. \tag{6–1}$$

Calculations were performed for $v_W = 2800$ m/min, which corresponds to $\omega = 58.33$ rad/s for $\eta = \eta_3$ (Figure 6). The results show that the rotating blade has a higher circumferential stress σ_θ, a lower contact stress q and a smaller contact region. The decrease in the contact stress near the blade's center ($\alpha = 0$) is about 0.07 MPa. This is somewhat larger than the magnitude 0.03 MPa predicted by the Lamé solution (B–7). The decrease in the peak value of the contact stress is about 0.5 MPa. However, even for this relatively low tension ($\sigma_\theta \approx 60$ MPa) in this thin blade the maximum effect of inertia is insignificant. Since the effect of inertia remains relatively constant for a given rotational speed, the effect is even more insignificant for higher tension (that is, for smaller values of η).

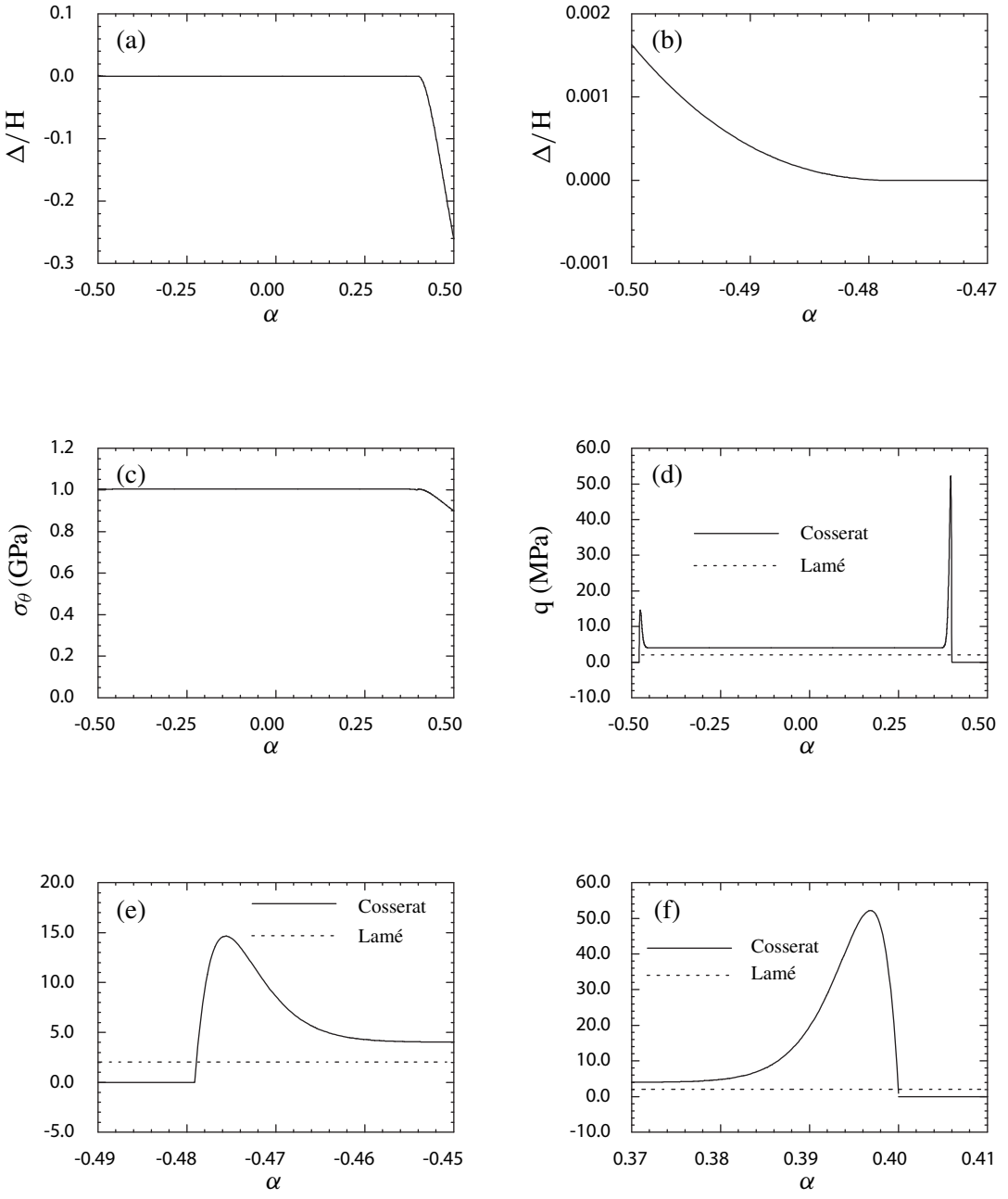

Figure 5. Plots of the radial gap Δ normalized by the thickness H, the circumferential stress σ_θ, and the contact stress q as functions of the normalized axial coordinate α for the case of large tension and a single contact region with the normalized misfit of the blade $\eta = -2.5$ and no angular velocity $\omega = 0$.

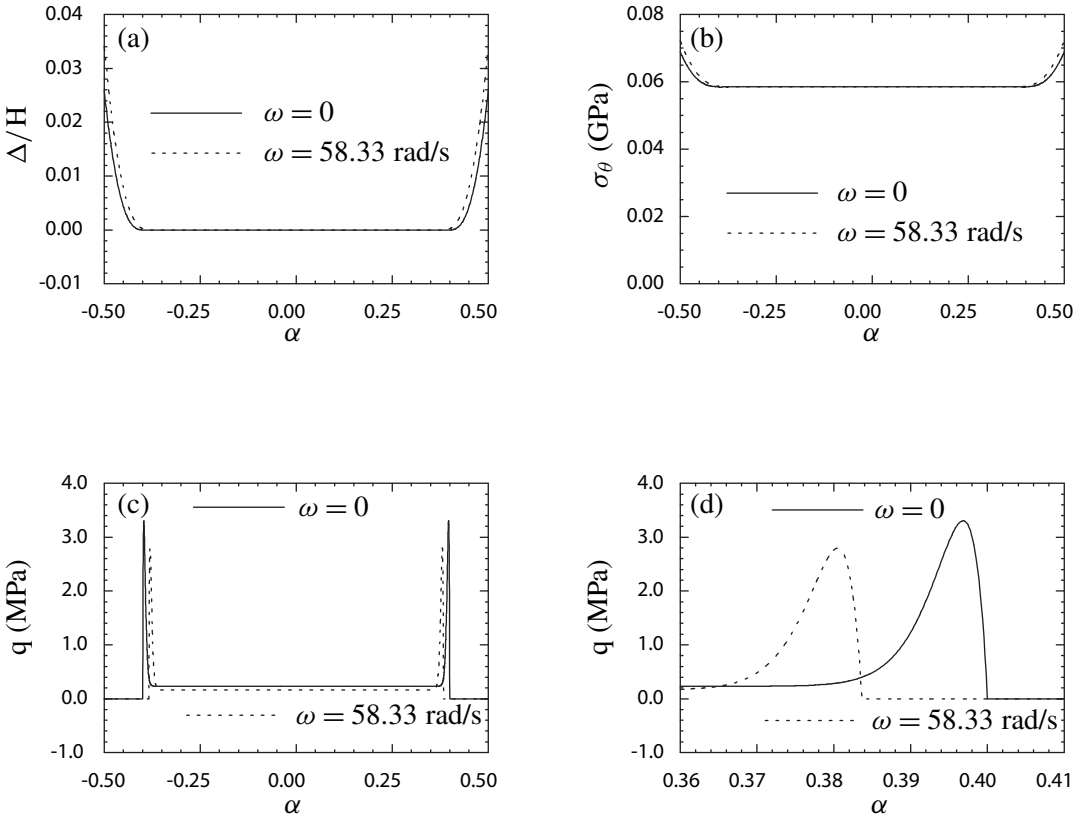

Figure 6. Effect of inertia. Plots of the radial gap Δ normalized by the thickness H, the circumferential stress σ_θ, and the contact stress q as functions of the normalized axial coordinate α for the point at which a single contact region reaches the edge of the wheel with the normalized misfit of the blade $\eta = \eta_3$ and with different angular velocities ω.

One of the difficulties in designing band saw blades is ensuring proper tracking of the blade on the wheel. As previously mentioned, the tensioning process and a crowned wheel are used to help control blade tracking [Lister and Schajer 1993; Wong and Schajer 1997; 2002]. The elastic effects of bending a plate into a circular cylindrical shell analyzed here also should influence tracking. It may be possible to exploit the facts that when the blade is free of contact it has a deformed shape (Figure 2a) and that this deformed shape causes stress concentrations when the blade is in contact (Figure 4c and Figure 5d). Specifically, if the wheel were crowned with slight curvature then it may be possible to adjust the curvature so that the blade would tend to hug the wheel (see Figure 7). The equations of Section 4 include a model for the tensioning process through the function $f_r(Z)$ and allow the wheel to have a crowned shape. Future research could explore the relative importance of these effects combined with the elastic effect that has been analyzed in this paper.

In conclusion, in this paper we model a band saw blade as an elastic plate that has been bent into a circular cylinder. Due to the Poisson effect, axial tension develops on the outer surface of the blade and

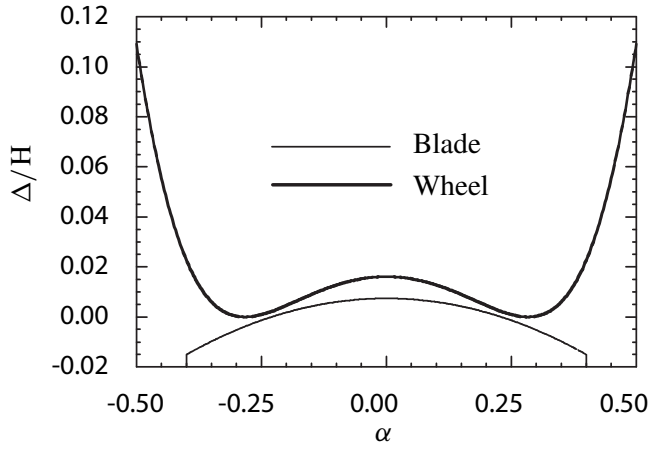

Figure 7. Sketch of a blade tracking on a crowned wheel.

axial compression develops on its inner surface. Consequently, end moments are required to maintain a right-circular cylindrical shape. The nonlinear equations of a Cosserat surface used to describe this process have been linearized and the resulting end moments are relieved, causing nonuniform deformation of the blade. It has been shown that this nonuniformity significantly influences the predictions of the value and distribution of the contact stress between the blade and the wheel even though the blade is thin. Also, it has been shown that the value of contact stress predicted by a simple Lamé-type solution is inaccurate and that the effects of the rotational speed of the wheel are negligible for typical operating conditions of thin wood-cutting saw blades.

Appendix A. Details of the solutions in the free and contact regions

The nonzero coefficients of $\{A^f_{ij}, B^f_{ij}\}$ associated with the free region are

$$
\begin{aligned}
&A^f_{11} = A^f_{22} = A^f_{33} = 1,\\
&A^f_{54} = (c_3^2 H),\\
&A^f_{65} = \Big(\frac{\nu^* c_3}{6(1-\nu^*)c_1 c_2^2} + \frac{1}{3c_1 c_3}\Big)\frac{H^2}{R},\\
&A^f_{66} = -\Big(\frac{1}{6(1-\nu^*)c_2^2} + \frac{\nu^*(1-2\nu^*)}{36(1-\nu^*)^2 c_1^2 c_2^4}\frac{H^2}{R^2}\Big)H^2,
\end{aligned}
$$

and

$$
\begin{aligned}
B^f_{14} &= B^f_{25} = B^f_{36} = -1,\\
B^f_{41} &= \left(4c_1c_3 + \frac{2c_1(c_3^2-c_2^2)}{c_3} + \frac{(c_1^2+2c_3^2)}{3(1-\nu^*)c_1^3c_3}\frac{H^2}{R^2} - \frac{2\rho_0^* H^2\omega^2 c_1}{\mu^*\pi^2 c_3}\right)\frac{1}{R},\\
B^f_{45} &= \left(\frac{4c_2c_3}{\nu^*} + \frac{2(1-\nu^*)(c_3^2-c_2^2)c_2}{\nu^* c_3} + \frac{c_2}{3\nu^* c_1^2 c_3}\frac{H^2}{R^2} - \frac{2\rho_0^* H^2\omega^2(1-\nu^*)c_2}{\mu^*\pi^2\nu^* c_3}\right),\\
B^f_{46} &= \left(-\frac{2\nu^*}{3(1-\nu^*)c_1c_2} - \frac{(1-2\nu^*)(c_3^2-c_2^2)}{6(1-\nu^*)c_1c_2^3} - \frac{c_3^2}{3c_1c_2^3}\right.\\
&\qquad \left. - \frac{(1-2\nu^*)}{36(1-\nu^*)^2c_1^3c_2^3}\frac{H^2}{R^2} + \frac{\rho_0^* H^2\omega^2(1-2\nu^*)}{6\mu^*\pi^2(1-\nu^*)c_1c_2^3}\right)\frac{H^2}{R},\\
B^f_{51} &= \left(4c_1c_3 + \frac{2c_1(c_3^2-c_2^2)}{c_3} - (3c_1^2-c_2^2)\frac{H}{R} + \frac{(c_1^2+2c_3^2)}{3(1-\nu^*)c_1^3c_3}\frac{H^2}{R^2}\right.\\
&\qquad \left. - \frac{(2c_1^2+3c_3^2)}{6(1-\nu^*)c_1^4}\frac{H^3}{R^3} + \frac{\rho_0^* H R\omega^2}{\mu^*} - \frac{2\rho_0^* H^2\omega^2 c_1}{\mu^*\pi^2 c_3}\right)\frac{1}{R},\\
B^f_{55} &= \left(\frac{4c_2c_3}{\nu^*} + \frac{2(1-\nu^*)(c_3^2-c_2^2)c_2}{\nu^* c_3} + 2c_1c_2\frac{H}{R} + \frac{c_2}{3\nu^* c_1^2 c_3}\frac{H^2}{R^2}\right.\\
&\qquad \left. - \frac{c_2}{3\nu^* c_1^3}\frac{H^3}{R^3} - \frac{2\rho_0^* H^2\omega^2(1-\nu^*)c_2}{\mu^*\pi^2\nu^* c_3}\right),\\
B^f_{56} &= \left(c_2c_3 - \frac{(6\nu^*-1)c_2^2 + (3-4\nu^*)c_3^2}{6(1-\nu^*)c_1c_2}\frac{H}{R} + \frac{\nu^* c_3(c_2^2-c_1^2)}{6(1-\nu^*)c_1^2c_2^3}\frac{H^2}{R^2}\right.\\
&\qquad \left. + \frac{(1-2\nu^*)}{36(1-\nu^*)^2c_1^3c_2^3}\frac{H^3}{R^3} + \frac{(1-2\nu^*)c_3}{36(1-\nu^*)^2c_1^4c_2^3}\frac{H^4}{R^4} + \frac{\rho_0^* H^2\omega^2(1-2\nu^*)}{6\mu^*\pi^2(1-\nu^*)c_1c_2^3}\frac{H}{R}\right)H,\\
B^f_{63} &= (c_3^2),\\
B^f_{64} &= \left(c_2c_3 + \frac{\nu^*(2c_1^2+c_3^2)}{6(1-\nu^*)c_1^2c_2c_3}\frac{H^2}{R^2}\right).
\end{aligned}
$$

The coefficients a_i^f in the characteristic Equation (5–6) are

$$
\begin{aligned}
a_0^f &= \left(B^f_{41}B^f_{55} - B^f_{45}B^f_{51}\right)B^f_{63},\\
a_1^f &= A^f_{65}\left(B^f_{46}B^f_{51} - B^f_{41}B^f_{56}\right) + A^f_{66}\left(B^f_{41}B^f_{55} - B^f_{45}B^f_{51}\right) - A^f_{54}B^f_{45}B^f_{63} + \left(B^f_{45}B^f_{56} - B^f_{46}B^f_{55}\right)B^f_{64},\\
a_2^f &= A^f_{54}\left(A^f_{65}B^f_{46} - A^f_{66}B^f_{45}\right).
\end{aligned}
\tag{A–1}
$$

The nonzero coefficients of $(A^c_{ij}, B^c_{ij}, C^c_i)$ associated with the contact region are

$$A^c_{ij} = A^f_{ij}, \qquad B^c_{ij} = B^f_{ij} \quad \text{(except for } i = 4\text{)},$$
$$B^c_{41} = \Big(1 + \frac{c_1}{2c_3}\frac{H}{R}\Big)\frac{1}{R}, \qquad B^c_{45} = \Big(\frac{(1-\nu^*)c_2}{2\nu^* c_3}\Big)\frac{H}{R},$$
$$B^c_{46} = -\Big(\frac{(1-2\nu^*)}{24(1-\nu^*)c_1 c_2^3}\Big)\frac{H^3}{R^2}, \qquad C^c_4 = -\Big(c_1 - \frac{H}{2R}c_3 - \frac{R_W}{R}\Big).$$

The coefficients a^c_i in the characteristic Equation (5–14) are

$$\begin{aligned} a^c_0 &= \big(B^c_{41}B^c_{55} - B^c_{45}B^c_{51}\big)B^c_{63}, \\ a^c_1 &= A^c_{65}\big(B^c_{46}B^c_{51} - B^c_{41}B^c_{56}\big) + A^c_{66}\big(B^c_{41}B^c_{55} - B^c_{45}B^c_{51}\big) \\ &\quad - A^c_{54}B^c_{45}B^c_{63} + \big(B^c_{45}B^c_{56} - B^c_{46}B^c_{55}\big)B^c_{64}, \\ a^c_2 &= A^c_{54}\big(A^c_{65}B^c_{46} - A^c_{66}B^c_{45}\big). \end{aligned} \tag{A–2}$$

Appendix B. Lamé solution

Within the context of small axisymmetric deformations relative to a coordinate system rotating with angular velocity ω, the steady state equations of motion can be written as

$$\frac{dT^*_{RR}}{dR^*} + \frac{T^*_{RR} - T^*_{\theta\theta}}{R^*} = -\rho^*_0\omega^2 R^*, \qquad \frac{dT^*_{ZZ}}{dZ} = 0. \tag{B–1}$$

For generalized plane stress the displacements are given by

$$u^*_R = u^*_R(R^*), \qquad u^*_\theta = 0,$$

and the constitutive equations for the nonzero stresses and the axial strain e_{ZZ} yield

$$\begin{aligned} T^*_{RR} &= \frac{2\mu^*}{(1-\nu^*)}\Big(\frac{du^*_R}{dR^*} + \nu^*\frac{u^*_R}{R^*}\Big), \\ T^*_{\theta\theta} &= \frac{2\mu^*}{(1-\nu^*)}\Big(\nu^*\frac{du^*_R}{dR^*} + \frac{u^*_R}{R^*}\Big), \qquad T^*_{ZZ} = 0, \\ e_{ZZ} &= -\Big(\frac{\nu^*}{1-\nu^*}\Big)\Big(\frac{du^*_R}{dR^*} + \frac{u^*_R}{R^*}\Big). \end{aligned}$$

In these equations a superposed $(*)$ is used to denote that the quantities are associated with the exact three-dimensional linearized theory.

The boundary conditions for a cylinder of mean radius R and thickness H to be in contact with a wheel of radius R_W with a free outer surface can be expressed as

$$u^*_R = R_W - R_1, \tag{B–2}$$

$$q_L = -T^*_{RR}, \qquad \text{for } R^* = R_1 = R\Big(1 - \frac{H}{2R}\Big), \tag{B–3}$$

$$T^*_{RR} = 0, \qquad \text{for } R^* = R_2 = R\Big(1 + \frac{H}{2R}\Big), \tag{B–4}$$

where q_L is the contact stress predicted by this Lamé solution and R is specified by (4–7). It can easily be seen that the equations of motion (B–1) are satisfied provided that

$$\frac{d^2u_R^*}{dR^{*2}} + \frac{1}{R^*}\frac{du_R^*}{dR^*} - \frac{u_R^*}{R^{*2}} = -\Big(\frac{\rho_0^*\omega^2(1-\nu^*)}{2\mu^*}\Big)R^*, \tag{B–5}$$

which admits the general solution

$$\begin{aligned}
u_R^* &= \Big(\frac{1-\nu^*}{1+\nu^*}\Big)A_1R^* + A_2\frac{R_1^2}{R^*} - \Big(\frac{(1-\nu^*)\Omega^2}{(3+\nu^*)}\Big)\frac{R^{*3}}{R_1^2},\\
T_{RR}^* &= 2\mu^*\Big(A_1 - A_2\frac{R_1^2}{R^{*2}} - \Omega^2\frac{R^{*2}}{R_1^2}\Big),\\
T_{\theta\theta}^* &= 2\mu^*\Big(A_1 + A_2\frac{R_1^2}{R^{*2}} - \Big(\frac{(1+3\nu^*)}{(3+\nu^*)}\Big)\Omega^2\frac{R^{*2}}{R_1^2}\Big),\\
\Omega^2 &= \frac{\rho_0^*\omega^2(3+\nu^*)R_1^2}{16\mu^*},
\end{aligned} \tag{B–6}$$

where the constants $\{A_1, A_2\}$ are determined by the boundary conditions (B–2)

$$\begin{aligned}
A_1 &= \Big(\frac{(1+\nu^*)}{(1-\nu^*)+(1+\nu^*)(R_2/R_1)^2}\Big)\Big(\frac{R_W}{R_1}-1\Big)\\
&\quad + \Big(\frac{(1+\nu^*)}{(3+\nu^*)}\Big)\Big(\frac{(1-\nu^*)+(3+\nu^*)(R_2/R_1)^4}{(1-\nu^*)+(1+\nu^*)(R_2/R_1)^2}\Big)\Omega^2,\\
A_2 &= \Big(\frac{(1+\nu^*)(R_2/R_1)^2}{(1-\nu^*)+(1+\nu^*)(R_2/R_1)^2}\Big)\Big(\frac{R_W}{R_1}-1\Big)\\
&\quad - \Big(\frac{(1-\nu^*)}{(3+\nu^*)}\Big)\Big(\frac{\big(-(1+\nu^*)+(3+\nu^*)(R_2/R_1)^2\big)(R_2/R_1)^2}{(1-\nu^*)+(1+\nu^*)(R_2/R_1)^2}\Big)\Omega^2.
\end{aligned}$$

It then follows that the contact stress is

$$q_L = 2\mu\Big(\frac{(1+\nu^*)\big((R_2/R_1)^2-1\big)}{(1-\nu^*)+(1+\nu^*)(R_2/R_1)^2}\Big)\Big(\Big(\frac{R_W}{R_1}-1\Big) - 2\Big(\frac{(1-\nu^*)+(3+\nu^*)(R_2/R_1)^2}{(1+\nu^*)(3+\nu^*)}\Big)\Omega^2\Big). \tag{B–7}$$

Nomenclature

a_0^f, a_1^f, a_2^f	coefficients of the characteristic equation in the free regions
a_0^c, a_1^c, a_2^c	coefficients of the characteristic equation in the contact region
$A^{1/2}$	scalar related to the shell's reference area
A_{ij}^f	matrix of the derivatives in the free regions
A_{ij}^c	matrix of the derivatives in the contact region
A_i	constants in the Lamé solution
B_1	auxiliary variable

B_2	auxiliary variable associated with the normalized thickness
B_{ij}^f	matrix of the linear coefficients in the free regions
B_{ij}^c	matrix of the linear coefficients in the contact region
c_1	circumferential stretch
c_2	axial stretch
c_3	radial stretch
c_j^f	coefficients of the eigenfunctions in the contact region
$\boldsymbol{C}$	right Cauchy–Green deformation tensor
C_i^c	vector in the contact region
$d^{1/2}$	scalar associated with the present configuration
$D^{1/2}$	scalar associated with the reference configuration
$\boldsymbol{d}_\alpha$	tangent vectors to the shell's present surface
$\boldsymbol{d}_3$	director in the present configuration
$\boldsymbol{d}^i$	reciprocal vectors to the present directors $\boldsymbol{d}_i$
$\boldsymbol{D}_\alpha$	tangent vectors to the shell's reference surface
$\boldsymbol{D}_3$	reference director which models a material fiber through the shell's thickness
$\boldsymbol{D}^i$	reciprocal vectors to the reference directors $\boldsymbol{D}_i$
c_j^f	coefficients of the eigenfunctions in the free regions
$\boldsymbol{e}_i$	rectangular Cartesian base vectors
$\boldsymbol{e}_r, \boldsymbol{e}_\theta, \boldsymbol{e}_z$	cylindrical polar base vectors
e_{ZZ}	axial strain in the Lamé solution
E^*	Young's modulus associated with small deformations
$\boldsymbol{E}$	Lagrangian strain tensor
$f_r(Z)$	function associated with the localized moment which models the tensioning process
$\boldsymbol{F}$	deformation gradient
H	reference thickness (in the $\boldsymbol{e}_1$ direction) of the rectangular plate
i	$\sqrt{-1}$
$\boldsymbol{I}$	unit tensor
$\boldsymbol{K}^{\alpha\beta}$	second order tensors associated with the energy of bending and torsion
L	referenced length (in the $\boldsymbol{e}_2$ direction) of the rectangular plate
m	mass per unit reference area
$m\boldsymbol{b}$	assigned force due to body force and contact stresses on the shell's major surfaces

$m\boldsymbol{b}^3$	assigned director couple due to body force and contact stresses on the shell's major surfaces
$\boldsymbol{m}^\alpha$	contact resultant couples on the shell's edges
m_θ^1	circumferential value of $\boldsymbol{m}^1$
m_r^2	radial value of $\boldsymbol{m}^2$
m_z^2	axial value of $\boldsymbol{m}^2$
q	normal contact stress (positive for compression) between the blade and wheel
q_L	contact stress in the Lamé solution
r	deformed radius of the shell's reference surface
R	auxiliary variable associated with the deformed radius of the cylindrical shell
R^*	radial coordinate in the Lamé solution
R_1, R_2	radii in the Lamé solution
R_W	radius of the wheel
t	time
$\boldsymbol{t}^\alpha$	contact resultant forces on the shell's edges
$\boldsymbol{t}^3$	intrinsic director couple
t_θ^1	circumferential value of $\boldsymbol{t}^1$
t_r^2	radial value of $\boldsymbol{t}^2$
t_z^2	axial value of $\boldsymbol{t}^2$
T_{RR}^*, $T_{\theta\theta}^*$, T_{ZZ}^*	stress components associated with the Lamé solution
u_r	radial displacement
u_z	axial displacement
u_R^*	radial displacement in the Lamé solution
u_θ^*	circumferential displacement in the Lamé solution
$\boldsymbol{v}$	velocity vector
v_W	blade's translational velocity
$\boldsymbol{w}_3$	director velocity
W	reference width (in the $\boldsymbol{e}_z$ direction) of the rectangular plate
$\boldsymbol{x}$	location of a material point in the present configuration
$\boldsymbol{X}$	location of a material point in the reference configuration
y_i^f	variables in the free regions
y_i^c	variables in the contact region

y_i^{cP}	vector associated with the particular solution in the contact region
y^3	director inertia coefficient
y^{33}	director inertia coefficient
Y_{1j}^f, Y_{3j}^f	eigenvectors in the free regions
Y_{1j}^c, Y_{3j}^c	eigenvectors in the contact region
z	deformed axial position of the shell's reference surface
Z	reference axial coordinate
α	normalized axial coordinate
α_1	value of $\alpha(<0)$ where the blade looses contact with the wheel
α_2	value of $\alpha(>0)$ where the blade looses contact with the wheel
α_W	normalized axial location of the wheel's edge
β	auxiliary variable
$\boldsymbol{\beta}_\alpha$	inhomogeneous deformation vectors
δ_r	radial director displacement
δ_z	axial director displacement
δ_j^i	Kronecker delta symbol
Δ	radial gap of the blade's inner surface relative to the wheel
η	normalized misfit of the inner radius of the cylindrical shell relative to that of the wheel
η_1	value of η for which the blade first contacts the wheel
η_2	largest value of η for which the blade first experiences two free regions and one contact region
η_3	smallest value of η for which the blade first experiences two free regions and one contact region with the edge of the contact region being the edge of the wheel $\alpha_2 = \alpha_W$
θ	angular coordinate
θ^α	convected Lagrangian coordinates
λ	eigenvalue
λ_1^f, λ_3^f	eigenvalues in the free regions
λ_{R1}^f, λ_{R3}^f	real parts of the eigenvalues in the free regions
λ_{I1}^f, λ_{I3}^f	imaginary parts of the eigenvalues in the free regions
λ_1^c, λ_3^c	eigenvalues in the contact region
λ_{R1}^c, λ_{R3}^c	real parts of the eigenvalues in the contact region
λ_{I1}^c, λ_{I3}^c	imaginary parts of the eigenvalues in the contact region

μ^*	shear modulus associated with small deformation
ν^*	Poisson's ratio associated with small deformations
ρ_0^*	reference mass density (mass per unit volume)
σ_θ	approximate value of the circumferential stress
Σ	strain energy of the shell per unit reference area
ϕ_r	radial component of the deformed director $\boldsymbol{d}_3$
ϕ_z	axial component of the deformed director $\boldsymbol{d}_3$
ϕ_j^f	eigenfunctions in the free regions
ϕ_i^c	eigenfunctions in the contact region
ω	angular velocity of the saw blade
Ω	normalized angular velocity of the saw blade

Acknowledgments

This research was partially supported by M. B. Rubin's Gerard Swope Chair in Mechanics and by the fund for the promotion of research at the Technion. M.B. Rubin would also like to acknowledge helpful discussions with G. Schajer related to the simplified model of the problem as a shell in contact with a wheel.

References

[Barcik 2003] S. Barcik, "Experimental cutting on the table band-sawing mashine", *Holz Roh Werkst.* **61**:4 (2003), 313–320.

[Chung and Sung 1998] Y. Y. Chung and C. K. Sung, "Dynamic behavior of the band/wheel mechanical system of industrial band saws", *J. Vib. Acoust.* (*Trans. ASME*) **120** (1998), 842–847.

[Damaren and Le-Ngoc 2000] C. J. Damaren and L. Le-Ngoc, "Robust active vibration control of a bandsaw blade", *J. Vib. Acoust.* (*Trans. ASME*) **122**:1 (2000), 69–76.

[Eklund 2000] U. Eklund, "Influencing factors on sawing accuracy in a bandsawmill", *Holz Roh Werkst.* **58**:1-2 (2000), 102–106.

[Gendraud et al. 2003] P. Gendraud, J. C. Roux, and J. M. Bergheau, "Vibrations and stresses in band saws: a review of literature for application to the case of aluminium-cutting high-speed band saws", *J. Mater. Process. Technol.* **135**:1 (2003), 109–116.

[Kong and Parker 2005] L. Kong and R. G. Parker, "Vibration of an axially moving beam wrapping on fixed pulleys", *J. Sound Vib.* **280**:3-5 (2005), 1066–1074.

[Le-Ngoc and McCallion 1999] L. Le-Ngoc and H. McCallion, "Self-induced vibration of bandsaw blades during cutting", *Proc. Inst. Mech. Eng. C J. Mech. Eng. Sci.* **213**:4 (1999), 371–380.

[Lister and Schajer 1993] P. F. Lister and G. S. Schajer, "The effectiveness of the light-gap method for indicating changes in bandsaw frequency and stiffness", *Holz Roh Werkst.* **51** (1993), 260–266.

[Lunstrum 1981] S. J. Lunstrum, "Circular sawmills and their efficient operation", Technical report, U.S. Department of Agriculture, Forest Service, State and Private Forestry, Madison, WI, 1981, Available at http://www.fpl.fs.fed.us/documnts/misc/circsaw.pdf.

[Lunstrum 1984] S. J. Lunstrum, "Balanced saw performance", pp. 16–37 in *Sawing technology: the key to improved profits*, Forest Products Research Society, Madison, WI, 1984. Also published as Technical report no. 12, U.S. Department of Agriculture, Forest Service, Forest Products Utilization, Madison, WI, 1985.

[Mote and Naguleswaran 1966] C. D. Mote and S. Naguleswaran, "Theoretical and experimental bandsaw vibrations", *J. Eng. Ind.* (*Trans. ASME*) **88** (1966), 151–156.

[Mote Jr. 1965] C. D. Mote Jr., "A study of band saw vibrations", *J. Franklin I.* **279**:6 (1965), 430–444.

[Murata et al. 2002] K. Murata, Y. Ikami, and K. Fujiwara, "Change in revolution speeds of band saw wheels and power consumption during sawing", *Bulletin of FFPRI (Forestry and Forest Products Research Institute)* **1**:2 (2002), 141–149.

[Naghdi 1972] P. M. Naghdi, "The theory of plates and shells", pp. 425–640 in *S. Flugge's Handbuch der Physik*, vol. VIa/2, edited by C. Truesdell, Springer, Berlin, 1972.

[Naghdi and Rubin 1989] P. M. Naghdi and M. B. Rubin, "On the significance of normal cross-sectional extension in beam theory with application to contact problems", *Int. J. Solids Struct.* **25**:3 (1989), 249–265.

[Rubin 2000] M. B. Rubin, *Cosserat theories: shells, rods and points*, Solid Mechanics and its Applications **79**, Kluwer, Dordrecht, 2000.

[Wong and Schajer 1997] D. C. Wong and G. S. Schajer, "Effect of wheel profile on bandsaw tracking stability", pp. 41–52 in *Proceedings of the 13th International Wood Machining Seminar* (Vancouver), 1997.

[Wong and Schajer 2002] D. C. Wong and G. S. Schajer, "Factors controlling bandsaw tracking", *Holz Roh Werkst.* **60**:2 (2002), 141–145.

Received 20 Dec 2005.

M. B. RUBIN: mbrubin@tx.technion.ac.il
Faculty of Mechanical Engineering, Technion - Israel Institute of Technology, 32000 Haifa, Israel

E. TUFEKCI: tufekcie@itu.edu.tr
Faculty of Mechanical Engineering, Istanbul Technical University, Gumussuyu TR-34437, Istanbul, Turkey